Development of a Laboratory Apparatus to Study the Thermal Degradation Behavior of Commercial Jet Engine Oils

by

Amanda Jean Neer

A thesis submitted to the Graduate Faculty of
Auburn University
in partial fulfillment of the
requirements for the Degree of
Master of Science

Auburn, Alabama
May 7, 2012

Keywords: jet engine oils, thermal degradation,
fume event, air contamination

Approved by

Ruel A. Overfelt, Chair, Professor of Materials Engineering
Jeff Fergus, Professor of Materials Engineering
Bart Prorok, Associate Professor of Materials Engineering

Abstract

Air quality on airplanes is a key priority of the Federal Aviation Association (FAA). It is suspected that, although rare, oil leaks in the engine can potentially allow contaminants into the air supply that is provided to the passengers in the cabin. Reliable and validated commercial sensors would enable the air quality on the airplane to be monitored. Before sensors can be utilized on airplanes a better understanding of the degradation behavior of jet engine oils is needed. Although a few previous studies have reported on the reaction products produced during thermal degradation of oil, the experimental set-ups used exhibited limited flexibility. Current technology, such as thermogravimetric analysis (TGA), can provide the precise data and information needed for understanding the thermal degradation behavior of jet engine oil, but such laboratory instruments are expensive, can only evaluate small sample sizes, and constrain the possible experimental protocols. The laboratory apparatus described in this thesis performs the same functions as a TGA but it is reasonably inexpensive, accommodates samples up to 2 g, and provides considerable flexibility in designing experimental protocols. The thermal degradation system consists of a microbalance, a cylindrical furnace, and a crucible to hold the sample. The system can be easily interfaced with other laboratory equipment such as custom sensor chambers or a Fourier Transform Infrared Spectrometer (FTIR). The modes of heat transfer of the thermal degradation system are characterized in this paper. Additionally, preliminary results of the thermal degradation behavior of Mobil Jet Oil II are reported.

Acknowledgments

I would like to express gratitude to Dr. Ruel A. Overfelt for his patience, compassion, and guidance throughout this learning process. Under his tutelage, I have learned much about the essential qualities of a good engineer. These lessons will leave a lasting impression on my career path.

Many thanks are due to my committee members: Dr. Fergus and Dr. Prorok for their support and for providing invaluable insight.

I also would like to express much appreciation to LC Mathison for all of his technical support and expertise. It was through his skills that this project was made possible.

I would also like to acknowledge my fellow group members: John Andress, Lance Haney, Shawn Yang, Naved Siddiqui, Wil Kilpatrick, and Briana McCall for their support, insight, and friendship.

Last, but certainly not least, I would like to recognize the tremendous amount of support, understanding, and encouragement that I have received from my family and friends. Through them I have grown into the person I am today.

This project was funded by the U.S. Federal Aviation Administration (FAA) Office of Aerospace Medicine through the National Air Transportation Center of Excellence for Research in the Intermodal Transport Environment (RITE), Cooperative Agreement 07-C-RITE-AU. Although the FAA has sponsored this project, it neither endorses nor rejects the findings of this Research.

Table of Contents

List of Tables

List of Figures

List of Symbols

A	surface area
a	constant
APU	auxiliary power unit
CO	carbon monoxide
CO_2	carbon dioxide
c_p	specific heat capacity
E_T	total thermal energy
F_{12}	view factor
FAA	Federal Aviation Administration
FTIR	Fourier Transform Infrared Spectrometer
GC/MS	gas chromatography/mass spectrometry
h	heat transfer coefficient
m	mass
NDIR	non-dispersive infrared
NO_x	nitrous oxides
O_2	oxygen
O_3	ozone
OD	outer diameter
Q_{conv}	heat transferred by convection

$Q_{s \rightarrow surr}$	heat transferred by radiation from the sample to the surroundings
T	temperature of sample
TCP	tricresyl phosphate
TGA	thermogravimetric analysis
T_s	temperature of sample
T_i	initial temperature
T_{surr}	temperature of surroundings
t	time
VOC	volatile organic compound
ε	emissivity
σ	Stefan-Boltzman constant
τ	thermal time constant

1. Introduction

The average person spent approximately 34 hours sitting in traffic according to a report by the Texas Transportation Institute in 2009. Sitting in traffic costs the economy about $115 billion a year and that figure is expected to grow [1]. In addition to traffic, road travelers also have to worry about unexpected construction delays. It is easy to see why many people might opt to take an airplane for long distance trips. Many airlines offer to let the passenger sit back and relax while flight attendants take care of their needs as they are jetted to their destination. As passengers dream of sunny beaches or meeting with loved ones and flight crew members work diligently to ensure the passengers have a restful journey, the last thing on anyone's mind should be the quality of the air in the cabin. However, the airlines have recently been receiving some bad press about poor cabin air quality that is suspected to have made passengers and crew members sick [2-6].

Poor air quality could potentially be caused by people on the airplane giving off metabolic odors and exhaling carbon dioxide, or possibly air contaminants from fluid leaks in the air supply system [7]. Potential sources of air contaminants include a variety of aircraft working fluids, such as de-icing fluid, hydraulic fluid, jet fuel or jet engine lubricants. These fluids can enter the airliner cabin through the bleed air supply from the engines during flight or from the auxiliary power unit (APU) during ground operations. This situation will be referred to as a "fume event" throughout the rest of this thesis.

Most commercial aircraft are powered by gas turbine engines with the turbofan engine being the most common type, shown on the far left of Figure 1.1. A modern turbofan jet utilizes the combusted and rapidly expanding pressurized gas to spin a turbine producing the mechanical power to drive the ducted by-pass fan producing propulsion forces [8-11]. The driveshaft assembly is lubricated with aircraft-grade grease or oil to prevent damage to the engine at the extreme operational temperatures and pressures. About 1/5 of the air that enters the engine goes through the core where some of it is extracted by bleed ports during the compression stage (denoted by H and I in Figure 1.1). The bulk of the air goes through the by-pass where most of the thrust is produced [7]. In the compression stage, the air can reach temperatures as high as 650°C. The air extracted from the bleed ports supplies hot compressed air to the bleed air system.

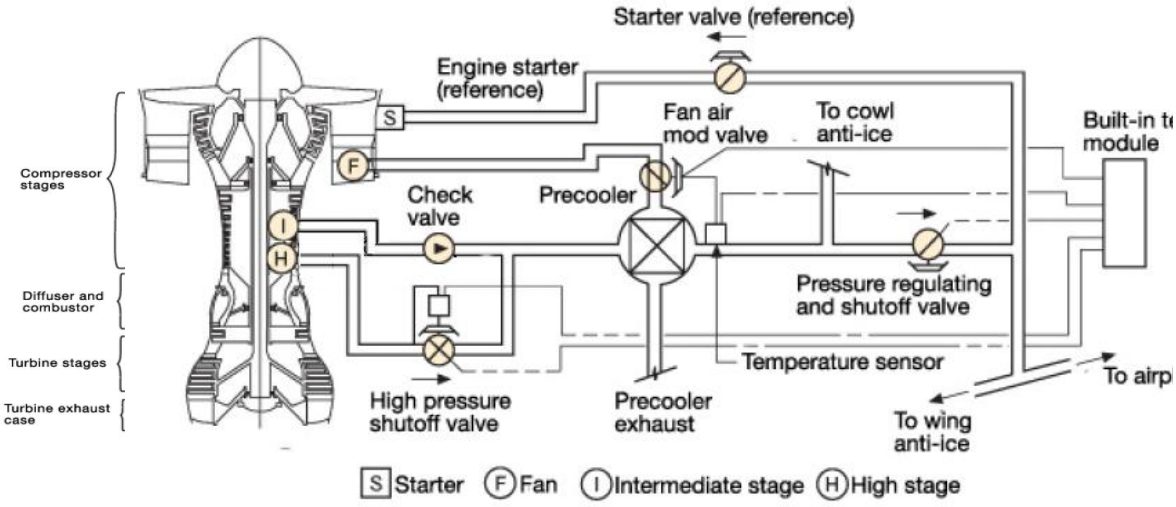

Figure 1.1: Diagram of the Bleed System of a Boeing 767 [7].

In the bleed air system, shown schematically in Figure 1.1, the air goes through a series of valves and a heat exchanger to bring the air to the proper temperature and pressure to power all pneumatic services on an airplane [7, 12]. Some of these services include the air-conditioning packs and cabin pressurization. In a typical bleed air system, the temperatures can range from 170˚C during ground operations to 350˚C during takeoff. (The aircraft is powered by an APU

during ground operations.) During cruise, the temperature of the bleed air system is approximately 250˚C [13]. The pressure of the bleed air from the engine can range from 1,170 kPa during takeoff to 340 kPa during cruise to 200 kPa during the initial descent[13].

Since the 1960s, jet engine oils and greases have been made of synthetic lubricants from the neopentyl polyol ester group. These esters were chosen because of their superior performance compared to petroleum-based lubricants, although additional additives are typically utilized for further enhancement of their lubricating properties. Van Netten [2, 3] and Winder et al [14] have found that these synthetic lubricants, when subjected to the high temperatures found in a jet engine, can release toxic gases. Some of these gases include carbon monoxide (CO), carbon dioxide (CO_2), and/or tricresyl phosphate (TCP) (a known neurotoxin, used as an anti-wear additive in engine oil). These contaminants can cause discomfort and in extreme cases threaten the health and safety of those exposed. Several cases have been reported by flight crew members of smoke, haze, and fumes entering the aircraft cabin and causing symptoms such as headaches and dizziness. In some cases, members of the flight crew were taken to the hospital for further treatment. Some of these events were linked to de-icing fumes and hydraulic fluid leaks in the engine [2].

The Federal Aviation Administration (FAA) has established regulations for how much carbon monoxide, carbon dioxide, and ozone (O_3) is safe in an aircraft cabin environment. The FAA has yet to pass any regulations regarding particulates, nitrogen oxides (NO_x), or volatile organic compounds (VOC), which can also be present in fume events involving lubricants and hydraulic fluids. Table 1.1 lists the air quality standards currently in place for aircraft [15]. Though there are standards to regulate what is safe for an aircraft, there are no regulations for actually monitoring the amount of pollutants on the aircraft.

Pollutant	Ambient Standard	Agency	Aircraft Standard	Agency
Ozone	0.12 ppm 1 –hr 0.08 ppm 8-hr	EPA NAAQS	0.1 ppm (sea level equivalent, time weighed average over 3-hr at >27,000 ft altitude) 0.25 ppm (sea level equivalent, at any time >32,000 ft altitude)	FAA(14 CFR 25.832)
Carbon monoxide	35 ppm 1-hr 9 ppm 8-hr	EPA NAAQS	50 ppm	FAA(14 CFR 25.831)
PM_{10}	150 $\mu g/m^3$ 24-hr	EPA NAAQS	None established	
$PM_{2.5}$	65 $\mu g/m^3$ 24-hr	EPA NAAQS	None established	
Nitrogen dioxide	0.05 ppm annual	EPA NAAQS	None established	
CO_2	None		5,000 ppm (sea level equivalent)	FAA (14 CFR 25.831)

ppm = parts per million by volume
PM_{10} = particulate matter less than 10 microns in diameter
$PM_{2.5}$ = particulate matter less than 2.5 microns in diameter
$\mu g/m^3$ = microgram per cubic meter

Table 1.1: Ambient and aircraft air quality standards [15].

Symptoms such as headaches, dizziness, and nausea will begin to manifest in passengers and the flight crew once CO concentrations are in the range of 70 to 220 ppm. Concentrations of 220 to 520 ppm will cause those on board to become incapacitated. Chances for survival at concentrations above 520 ppm are greatly lessened [16, 17]. A study by the National Air Pollution Control Administration (1970) found that exposure to 50 ppm of CO for 90 minutes will impair time-interval discrimination and visual function [18]. These findings and recent fume events on airplanes have placed pressure on the FAA to pass regulations that require monitoring the air quality on airplanes. In order for the FAA to make informed decisions when passing such regulations, an understanding of how the various aircraft working fluids degrade at elevated temperatures is necessary.

Over the past decade, several researchers have studied the thermal degradation behavior of various brands of lubricating oils as well as other types of aircraft working fluids. Thermogravimetric analysis (TGA) is a method used commonly to understand the thermal and

physical changes the oils experience when they degrade at high temperatures [2, 19-23]. TGA involves using a microbalance and a furnace to measure mass changes of a sample as it is being heated at a constant rate. With TGA it is possible to control the atmosphere around the sample during the heating process and the technique is very sensitive to mass loss. However, there are also disadvantages to using TGA to analyze the thermal properties of a sample. TGA can only analyze sample sizes up to 20 mg, and there is no contact between the thermocouple and the sample [24, 25]. Sample sizes this small may not be representative of the bulk oil properties. More importantly, larger sample sizes would enable various droplet surface area to volume ratios to be investigated. Also, it is useful to be able to correlate mass changes of the oil to specific temperatures of the oil itself. A laboratory system is needed that can address these concerns as well as perform the functions of the TGA.

In this study, a laboratory apparatus has been developed to evaluate the thermal degradation behavior of commercial jet engine oils at various temperatures. This apparatus is capable of characterizing the temperature as well as the mass of the oil simultaneously with a fair amount of accuracy. Not only was the system inexpensive to build compared to the price of purchasing a new TGA, but it also made it easier to control various operational parameters of the system, i.e. weighing functions, thermocouple placement, etc. The balance makes it possible to analyze very small sample sizes on the order of thousandths of a gram up to 2 grams. In addition to having a control thermocouple in the furnace, another thermocouple is placed in the sample. The heat transfer mechanisms of the apparatus have been characterized and a model has been developed. The goal of this research is to develop and characterize an apparatus that can be exploited in future research to further understand how jet engine oils degrade. This information will help guide the future work to determine the best method to detect fume events on airplanes.

2. Literature Review

It is essential to have an understanding of the chemical degradation mechanisms of jet engine oils at elevated temperatures in order to make informed decisions on any sensors that could be put on airplanes to detect fume events. Information such as when smoke begins to appear and at what temperature it first appears is important, because that can potentially indicate the formation of CO detectable by commercial sensors. A few different methods have been utilized by previous researchers. It seems that some of these methods were not very reliable and that others could benefit from wider experimental capabilities. The studies done in the past have merely heated the oil and noted smoke formation and oil color change while measuring the evolved gases. This study describes a laboratory apparatus that can do all the things done by previous researchers as well as measure the mass change and record direct measurements of the oil temperature during degradation.

This literature review is divided into three sections. The first section is an overview of methods that have been used by other researchers to evaluate the thermal degradation behavior of jet engine oils, namely thermogravimetric analysis (TGA). The second section discusses the findings of other researchers in the field of thermal degradation of jet engine oils. The third section summarizes the limitations of the previous techniques used and discusses how this research addressed these limitations.

2.1 Experimental Techniques Used to Thermally Degrade Jet Engine Oil

Many techniques have been utilized by various researchers to analyze the thermal degradation behavior of jet engine oils. They vary from complex thermogravimetric analysis

(TGA) systems connected to Fourier Transform Infrared (FTIR) spectrometers or gas chromatography/mass spectrometry (GC/MS) to simpler systems consisting only of a heating element and a crucible. In this section, TGA systems will be discussed in detail.

TGA is a popular technique because it requires little set up and working instruments can be purchased from reputable manufacturers. TGA measures the weight change of a sample as a function of temperature/time. The mass change rate as a function of time can be used to interpret the reaction kinetics samples experience and quantify any evolved and/or absorbed gases [24-26]. For example, TGA can be used to evaluate loss of water, loss of solvent, decarboxylation, pyrolysis, oxidation, etc.

TGAs come in a variety of models that can be customized by the user. The set-up modules may vary slightly, but the basic operation remains the same. This section describes a typical set-up that is common to most TGAs and is shown schematically in Figure 2.1. TGAs consist of a microbalance, a furnace, and a crucible to hold the sample. Quartz-crystal microbalances in a TGA typically have a maximum sample size of 50 mg due to the dimensional requirements for the crucibles and the furnace. The microbalance is electronically compensated to account for movement of the crucible as the sample begins to gain or lose weight and is extremely sensitive to mass loss. The furnace is raised and lowered around the stationary crucible. The typical maximum operating range is from room temperature to 1000˚C and typical heating rates range from 10°C/min to 20°C/min. The crucible is typically porcelain or platinum because these materials are very stable at high temperatures. The crucible normally sits atop the microbalance and the furnace is lowered into position, though in some models the crucible may be attached to the microbalance from below. The sample temperature is measured by a thermocouple at the sample crucible but not in the sample itself. Some TGAs are equipped with a

purge gas outlet that can be coupled to an FTIR or GC/MS. TGAs can often be set for vacuum or select atmospheres, i.e. nitrogen, air, and under a range of pressures. Modern TGAs are carefully controlled by computer.

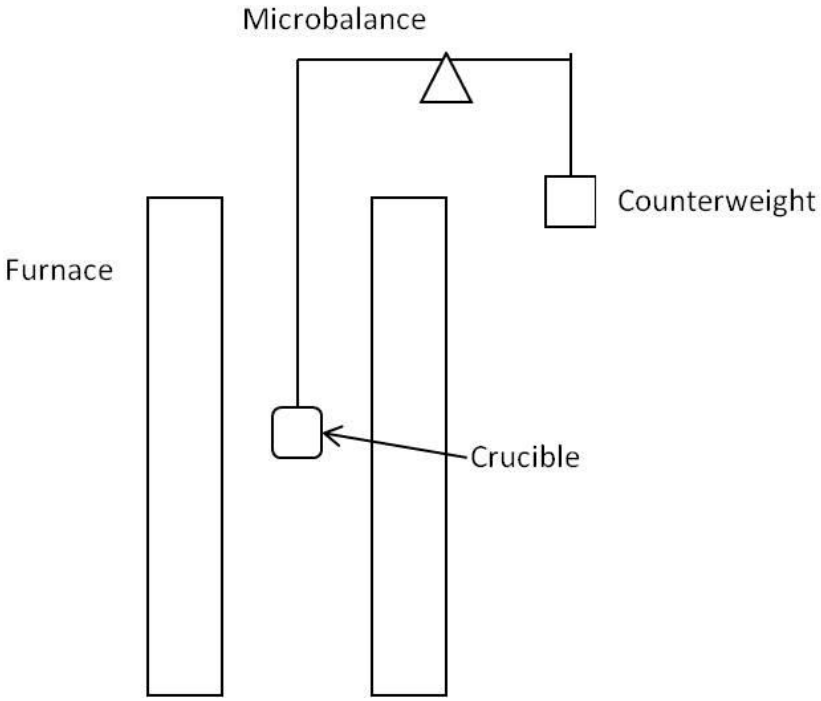

Figure 2.1: Schematic of TGA arrangement.

In summary, TGA is an excellent technique for characterizing mass changes as a function of temperature or time for many samples. Specifically it makes it possible to understand oxidation reactions and compositions of samples and many other reaction behaviors. TGAs consist of a microbalance, a furnace, and a crucible to hold the sample. It offers many experimental capabilities by being able to be connected to FTIR and GC/MS. Not many studies have performed TGA on oil; most have used simple set-ups.

2.2 Thermal Degradation Behavior of Jet Engine Oil

Van Netten et al evaluated a range of hydraulic fluids and jet engine oils [2-4] utilizing a small 5 cm X 5 cm piece of aluminum foil to hold the fluid sample during heating by a ceramic

hot plate. A thermocouple was used to monitor the temperature of the hot plate. Gases were evolved in a 250 L stainless steel chamber equipped with a multigas monitor TMX-412 (Industrial Scientific Corporation, Oakdale, PA) to measure NO_2, oxygen (O_2), and CO. Additionally, a YES-204A monitor (Young Environmental Systems, Richmond, B.C., Canada) was also in the chamber to measure temperature, relative humidity, and CO_2 concentration [4]. The hot plate with the aluminum foil holder containing the test fluid was first placed into the chamber and then heated to 525°C at a rate of 10°C/min. Samples were then isothermally held for 1 minute at 525°C before being allowed to cool to room temperature. Air sensors began recording the ambient air before the oil was inserted into the test chamber. Also, air samples were retrieved from the chamber for later analysis by GC/MS.

Van Netten et al [2] noted that the Mobil 254 jet engine oil was initially dark blue in color at room temperature. When the hot plate reached approximately 275°C white smoke began to form and the oil turned a dark brown-orange color. At 400°C, it was noted that charring of the oil began to occur and the white smoke continued to form. At 500°C, some charred material remained on the aluminum foil sheet. Approximately 102.5 ppm CO and 460 ppm CO_2 were detected at 525°C [2]. Air sample results from GC/MS analysis indicated the presence of TCP isomers as well as volatile derivatives of pentane, hexane, and octane during degradation of Mobil 254 jet engine oil.

Castrol 5000 was orange in color at room temperature and began producing white smoke at approximately 285°C. Darkening of the oil began at 310°C and charring was observed at 350°C. At the end of the experiment only charred brown material remained. The CO_2 sensor measured roughly 510 ppm CO_2. The CO sensor detected approximately 140 ppm CO from Castrol 5000 [4].

Van Netten et al [2] noted that Exxon 2380 was light orange in color at room temperature. At about 275°C, the oil began producing white smoke. Darkening of Exxon 2380 began at 300°C and charring was observed at 310°C. At the end of the experiment only charred brown material remained. The CO_2 sensor measured roughly 510 ppm CO_2 and the CO sensor measured about 120 ppm CO [4]. GC/MS analysis of the gases produced by degrading Castrol 5000 and Exxon 2380 indicated that the components of the evolved gases were very similar to one another. NO_2 was not detected during degradation of any of the oil samples.

Crane et al [27] also evaluated Exxon 2380. These authors utilized a custom-built combustion chamber to analyze evolved gas samples. The Crane et al [27] chamber had a much smaller total volume of approximately 12.6 L. Three milliliters of sample was placed in a semi-cylindrical quartz combustion boat, 7.5 cm long by 4 cm wide. The boat was placed in a horizontal quartz tube with a 5 cm diameter and was 33 cm long. Two semi-cylindrical heating elements encapsulated the quartz tube and the temperature was controlled by a thermocouple placed in one of the heating elements. The sample was continuously heated from room temperature until only charred material remained. Exxon 2380 began producing a measurable amount of CO around 306°C at roughly the same time the authors noticed an increase in visible smoke production. At 344°C, CO concentration was measured at 5,000 ppm CO and at 350°C only charred material remained. The solid char continued to produce CO up to 530°C. When the oil was exposed to 600°C, the authors reported a much higher CO level of 17,000 ppm CO.

Bartl et al [23] evaluated pentaerythritol derivatives (the base component of jet engine oils) using TGA. These researchers heated 10 mg of pentaerythritol from room temperature to 1000°C at 10°C/min in air. Figure 2.2 shows TGA and DTA (differential thermal analysis) data of a pentaerythritol derivative in air. The weight change data shows that the sample began to lose

mass at approximately 275°C, which is roughly the temperature Van Netten et al [2] began seeing the oils generate smoke. Also DTA data indicates sample heating due to exothermic reactions (i.e., burning) in the oil as the oil degrades. The first peak at approximately 350°C corresponds to an oxidation reaction in which volatile reaction products are produced. The second peak at about 570°C is due to the oxidation of the carbonaceous fraction to CO and CO_2. This can be roughly correlated to the CO and CO_2 evolution reported by Van Netten at 525°C.

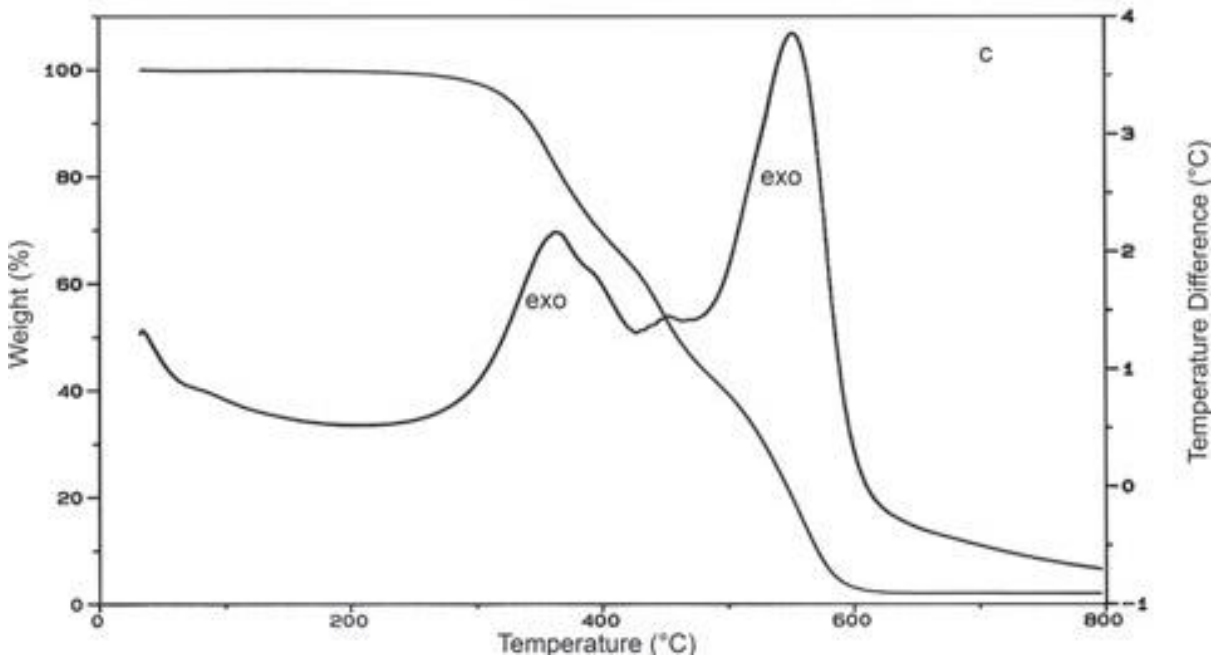

Figure 2.2: TGA and DTA plot of pentaerythritol derivative in air [23].

Van Netten et al [2, 4] and Crane et al [27] noted the temperatures at which the oils began to smoke. Van Netten reported that Mobil 254 and Exxon 2380 began producing smoke at about 275°C. Castrol 5000 began producing smoke at 285°C. Crane reported that Exxon 2380 began producing smoke at 306°C. Differences in the temperature that Exxon 2380 began smoking may be attributed to the different arrangements used. Van Netten et al used a hot plate and so the oil was only being heated from the bottom. The thermocouple that was used to record the

temperature was simply laid on top of the hot plate also and it is possible that some heat loss due to the surrounding air may have occurred resulting in a lower temperature reading. Crane et al placed the oil in a ceramic boat in a quartz tube that was surrounded by a heating element. This method provided the sample with better uniform heating and additionally the thermocouple was embedded inside the furnace reducing the amount of heat loss to the surroundings. The slight differences between the oils evaluated by Van Netten can possibly be attributed to variations in the components of the oils.

2.3 Limitations of Previous Research

One limitation of much of the previous research involves the actual temperature of the oil when it is being degraded. Having a thermocouple directly in the oil would enable more reliable characterization of the oil temperature in the event that it lags the heating element during heat-up or leads the heating element during exothermic reactions. Such data are important to precisely understand the thermal degradation reaction kinetics. Reliable temperature measurements would also make it possible to calculate convective heat transfer coefficients. This would also lead to a better understanding of how the oil is degrading.

In addition, all of the previous studies evaluated relatively small sample sizes. Crane et al used about 3 g of oil. Larger sample sizes would enable various oil droplet surface area to volume ratios to be used and allow oil degradation to be analyzed using standard combustion techniques.

In summary, none of the studies reviewed directly measured the temperature of the oil as it was heating. This is important for understanding the degradation behavior of the oil. The studies in this review evaluated relatively small sample sizes. Larger sample sizes may provide a better idea of bulk oil behavior during degradation. Mass change was not taken into account by

Van Netten and Crane. Recording mass changes during degradation should enhance our understanding of the degradation behavior of the oil.

3. Experimental Procedures and Analytical Techniques

3.1 Thermal Degradation System

A laboratory apparatus has been developed to thermally degrade aircraft working fluids. The thermal degradation system was used to degrade jet engine oils at various elevated temperatures. This system, shown in Figure 3.1, incorporated a microbalance from which the fluid samples were suspended into a cylindrical ceramic fiber furnace. This arrangement is similar to a TGA except that larger samples and unique experimental protocols can be investigated. The microbalance – furnace assembly was housed within a 50 L bell jar to contain any evolved gases that were produced during experiments. The entire thermal degradation system was further enclosed by a custom built fume hood to contain any possible leaks in the system for additional safety.

There were two plastic tubes of 12 mm inner diameter and 61 cm length on either side of the furnace that drew room temperature air from the room into the top of the bell jar where the microbalance was housed. The airflow direction is indicated by the blue dashed arrows in Figure 3.1. The air flow from the plastic tubes was directed around the microbalance and then through a hole beneath the microbalance, and down the length of the furnace passing over the suspended crucible assembly where any evolved gases or smoke could be entrained within the air stream. The furnace was hollow in the center and open on both ends allowing air to flow all the way through to an opening in the base plate that is connected to a six-way cross. A six-way cross at the bottom allowed the air stream to be coupled to other laboratory analysis equipment, i.e.

unique sensor chambers, a Fourier Transform Infrared spectrometer (FTIR), etc. The air stream was powered by an 11,600 sccm vacuum pump during and after the experiments.

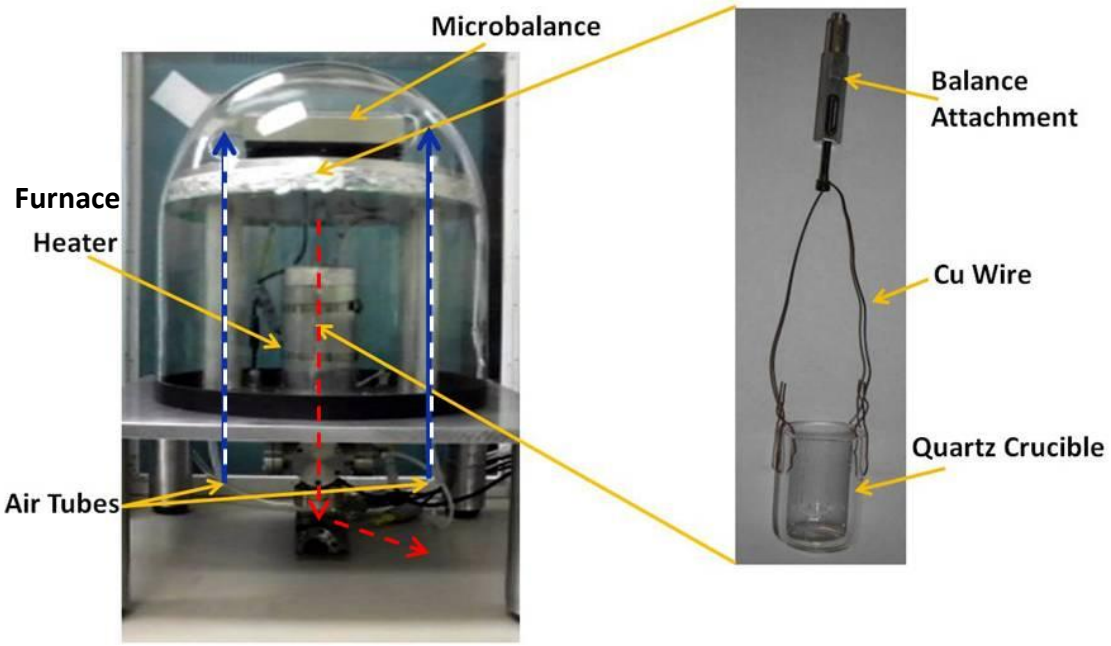

Figure 3.1: Thermal Degradation System.

1) Microbalance

The thermal degradation system utilized a Scientech SM124D microbalance (Boulder, CO) to measure changes in mass of the experimental working fluid during thermal exposures. The microbalance had a dual range mode: one with a maximum capacity range of 40 g and the other with a maximum capacity of 120 g. For all the experiments in this study, the 120 g range was used. The microbalance enabled measurements of mass within ±0.6 mg over the experimental mass range. The microbalance had a "below balance" or a "hang down" weighing mechanism that enabled the crucible suspension assembly to be inserted into the furnace while characterizing the mass. Balance calibration was checked and verified prior to any evolved gas experiments using calibration weights of known mass. The balance calibration was verified

every day that the balance was used to ensure minimal error in the mass measurements. On average, the measured values from the balance tended to be slightly lower than the reported values for the calibration weights, but agreement was typically within 0.027% of the reported value. The microbalance was controlled externally by a computer. All of the data recorded from the microbalance were analyzed with Microsoft Excel 2007®.

The microbalance was located approximately 8 cm above the furnace. A 2.5 cm layer of ceramic fiber board was used to insulate the balance from the furnace underneath. The fiber board was wrapped in aluminum foil and then sandwiched between two layers of aluminum, 12 mm thick on top and 1.5 mm thick on bottom. The aluminum and fiber board were supported by four aluminum legs approximately 2.5 cm in diameter. The crucible was attached to the microbalance from below and hung through the same hole that air was drawn through as discussed earlier. There were alignment holes on the bottom of the legs that matched pegs in the base plate to ensure repeatable placement. Finally, a 1.5 mm thick rubber gasket formed a compression seal between the 12 mm thick microbalance support plate and the inside of the bell jar to ensure that air flow was always from the microbalance area through the crucible hang down hole, through the furnace and out of the system to protect the microbalance from possible contamination during thermal degradation experiments.

2) Furnace

A cylindrical ceramic fiber furnace (Watlow, Chicago, IL) was used to heat the working fluid samples to the desired temperatures. The heating elements were composed of a high temperature iron-chrome-aluminum alloy and were insulated by an alumina-silica compound. The operating parameters of the furnace, i.e. temperature set point and heating rate, were adjusted by a furnace controller (Watlow, Chicago, IL). The furnace had an outer diameter of 10

cm, an inner diameter of 5 cm and was approximately 15 cm in height. The maximum operating temperature of the furnace was 2200˚C. A 2 mm diameter through hole was fabricated in the furnace side about 7 cm from the top for location of a furnace control thermocouple.

Type K thermocouples (Omega Engineering Inc., Stanford, CT), insulated with ceramic tubes and woven ceramic fiber, were used for all temperature measurements. The reliability of the thermocouples was checked by measuring the boiling point of water. The thermocouple measurements agreed within 1% of the boiling point of water. A thermocouple was placed in the experimental fluid sample for all thermal degradation measurements and was also attached securely to the bottom of the microbalance support structure to eliminate inadvertent contact between the thermocouple and the hang down assembly and to minimize movement of the thermocouple within the fluid sample. All data recorded from the thermocouples were analyzed using Microsoft Excel 2007®.

3) Working Fluid Samples: Jet Engine Oils

Two commercial jet engine oils were selected for this study: Aeroshell 560 (Shell Aviation) and Mobil Jet Oil II (ExxonMobil) because they are the most commonly used in the airline industry. The properties for each of the oils are given in Table 3.1. The base component of these jet engine oils is 95% pentaerythritol. The oils also contain 2 – 4% antioxidants, such as N-phenyl-2-naphthylamine and 1 – 3% antiwear additives, such as tricresyl phosphate. In addition, corrosion inhibitors, rust inhibitors, and anti-foaming agents are also typically added to enhance the performance of the oils [14, 28, 29]. It was assumed that both of the oils had the same heat capacity because they have similar base components. The oils were stored in air tight containers at room temperature.

	Aeroshell 560	Mobil Jet Oil II
Color	amber	amber
Density [g/cm^3]	0.996	1.00
Flash Point [˚C]	260	270
Auto ignition Temp [˚C]	320	404
Heat Capacity @constant P [J/Kg K]	2130	2130

Table 3.1: Manufacturers' data on commercial jet engine oils [28,29].

3.2 Experimental protocol to evaluate heat transfer mechanisms

Three materials were used to investigate the heat transfer mechanisms occurring in the thermal degradation system. Initially, a 6061 aluminum slug, shown in Figure 3.2, was used to develop heat transfer models because its thermal properties have been well-documented [30-32]. The models developed were then applied to fused quartz and stainless steel crucibles, also shown in Figure 3.2. These crucibles were planned for usage with the oil samples. The quartz crucible had a volume of 20 milliliters while the steel crucible had a volume of 50 milliliters.

Figure 3.2: Steel crucible, Al slug, quartz crucible used in the experiments.

Each of the crucibles was attached by a copper wire through two holes on either side and then suspended in the center of the furnace as discussed in section 3.1. The aluminum slug had a through-hole in the center to allow for the placement of a thermocouple. For the experiments with the crucibles, the thermocouple was placed in contact with the crucible bottom and positioned as close to the center of the crucible bottom as possible. Figures 3.3, 3.4, and 3.5 show cross-sectional views of the positions of the aluminum slug, the quartz crucible, and the steel crucible in the furnace during the heating portion of the experiments.

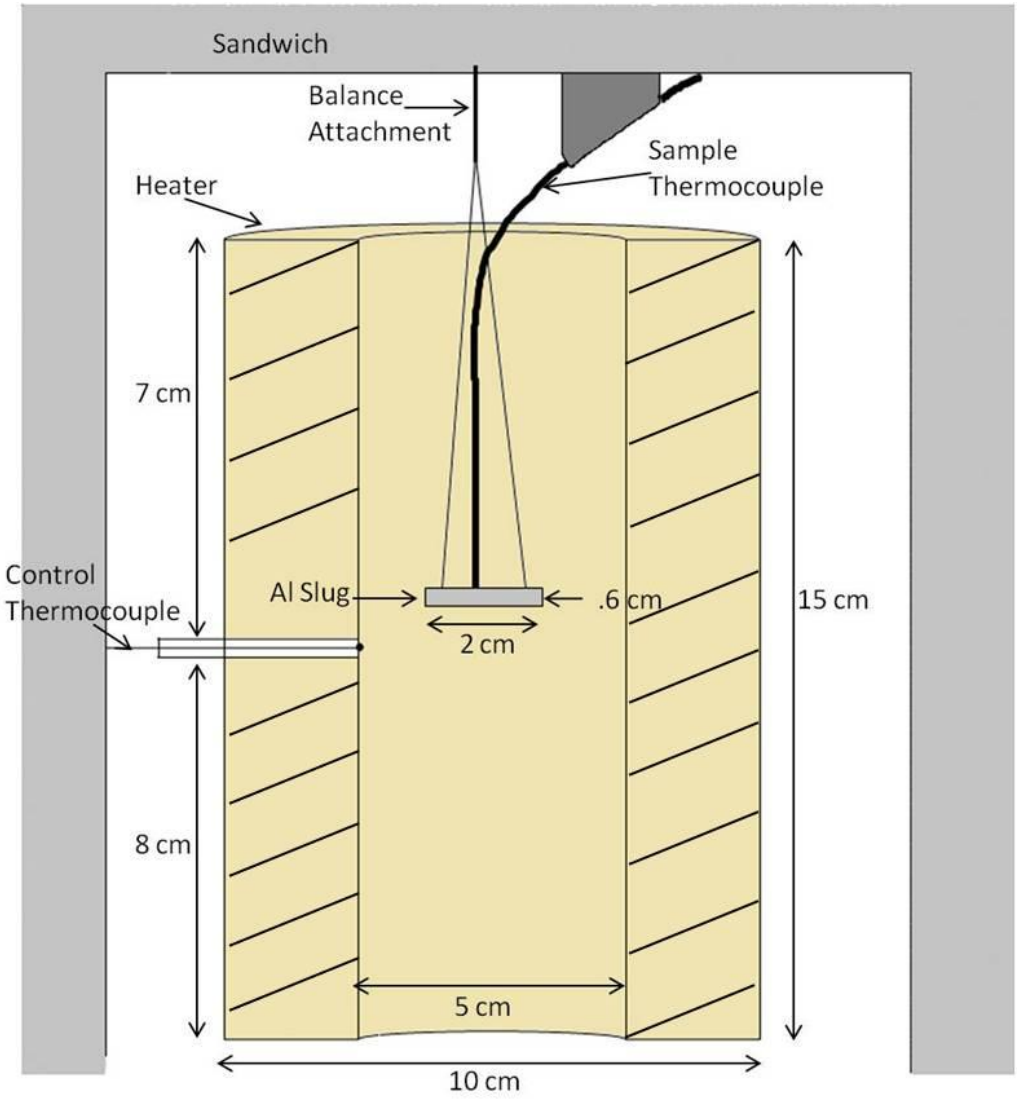

Figure 3.3: Cross-sectional view of the position of Al slug in furnace.

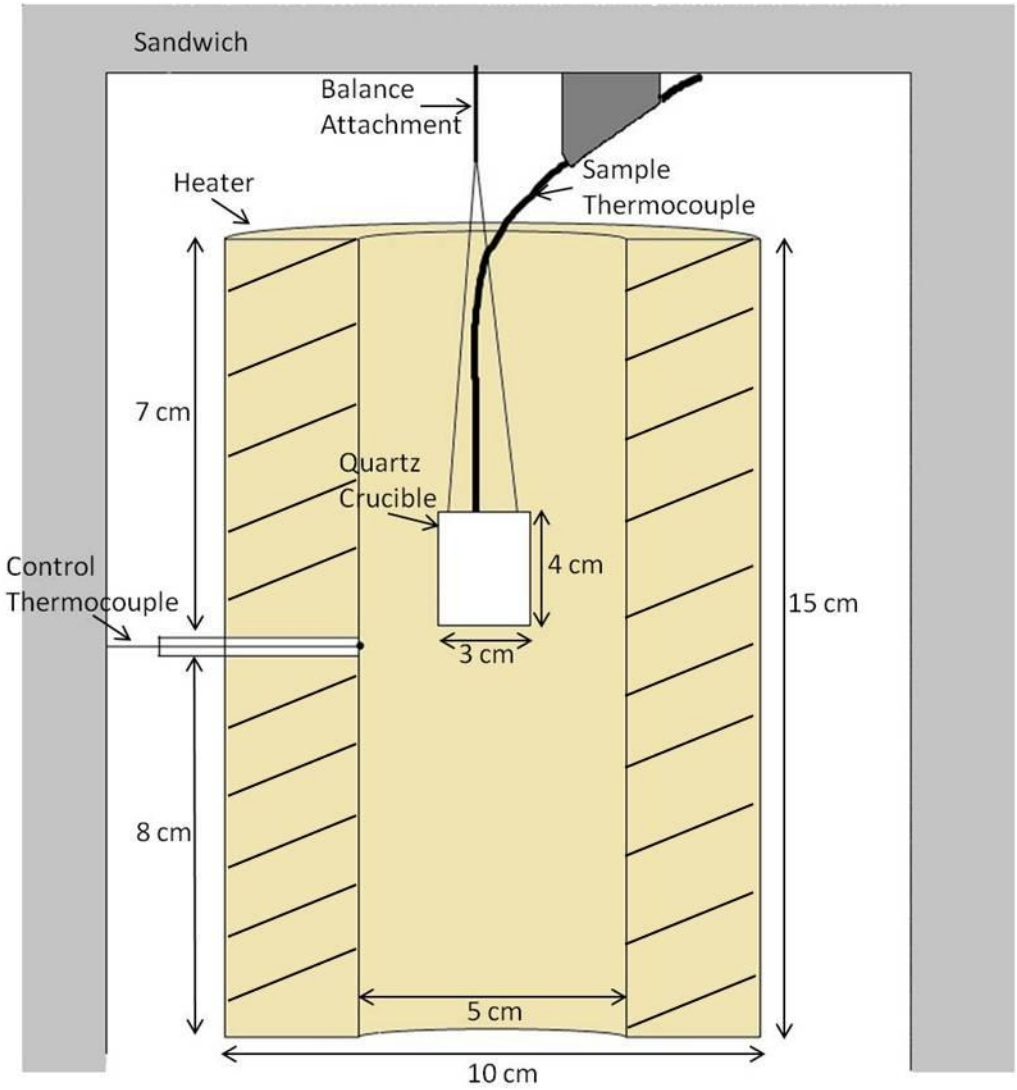

Figure 3.4: Cross-sectional view of the position of quartz crucible in furnace.

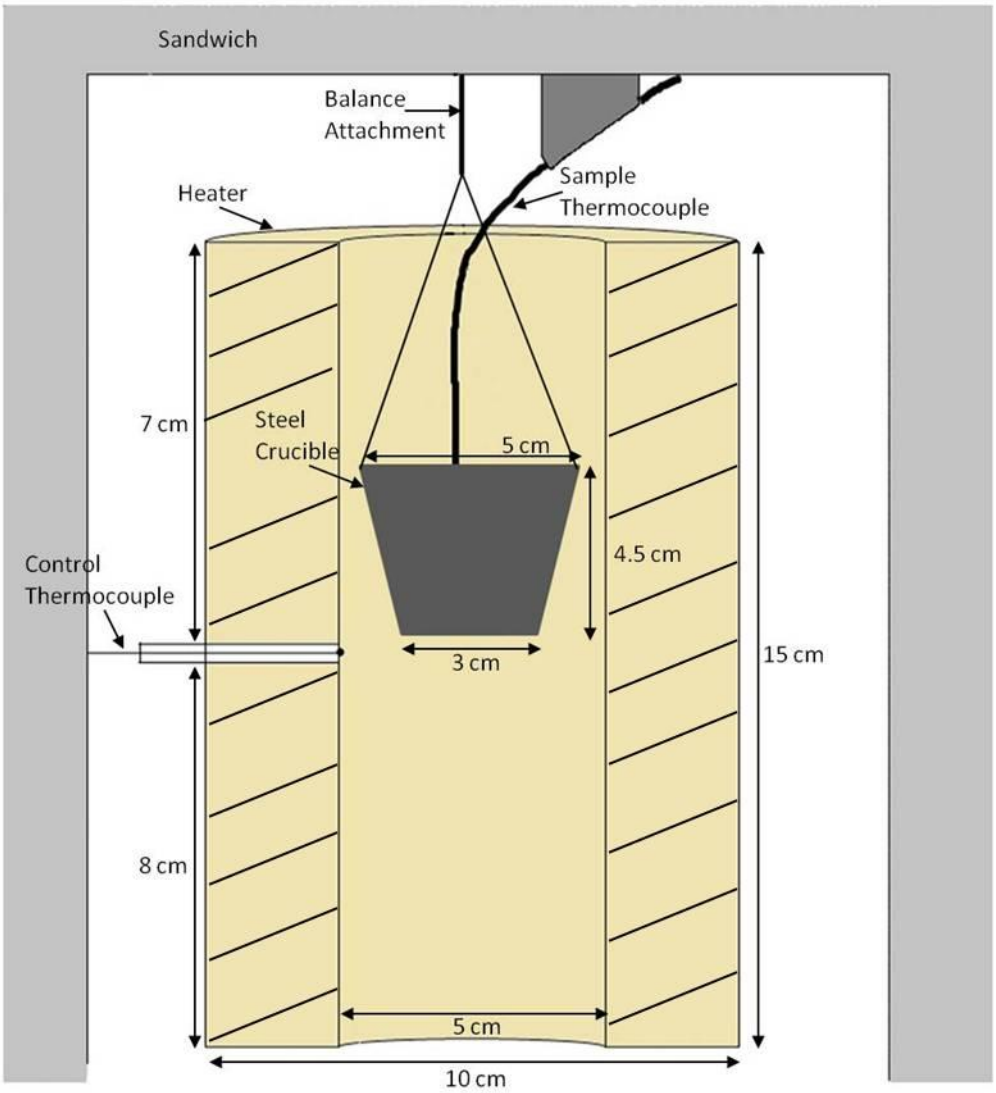

Figure 3.5: Cross-sectional view of the position of steel crucible in furnace.

The experimental protocol for the heat transfer experiments was carried out with the following steps:

1. The appropriate crucible or aluminum slug was attached to a copper wire and suspended from the microbalance support assembly.
2. The furnace was preheated to the desired temperature.
3. The furnace was allowed to stabilize (approximately one hour).
4. The appropriate crucible or aluminum slug was placed in the furnace for one hour.
5. Temperature measurements were recorded at a rate of 1 Hz for both heating and cooling.
6. The system was allowed to cool to room temperature.

Furnace set point temperatures of 300, 350, 400, 450, and 500°C were used for these heat transfer measurements. Each of the samples was evaluated at each of the set points and repeated to ensure repeatability. These temperatures were chosen to represent the range of exposure temperatures anticipated for the various working fluids of interest.

3.2.1 Experimental Arrangement to evaluate temperature gradients in crucibles

The temperatures in the center and of the outer diameter of the crucibles were measured to examine the temperature gradients across crucibles containing one milliliter of Aeroshell 560 Turbine oil. The purpose of this experiment was to determine the sensitivity of thermocouple location on the crucible temperature measurements. The experimental protocol for characterizing the crucible temperature gradients was carried out with the following steps:

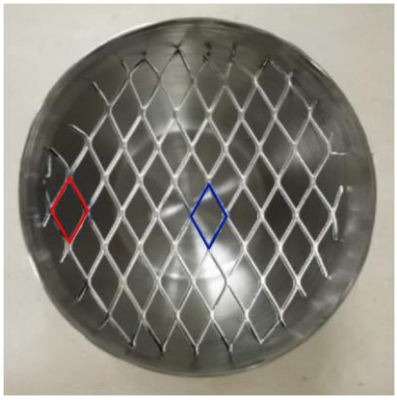

Figure 3.6: Holder to hold thermocouples in place.

1. One milliliter of Aeroshell 560 Turbine Oil was

placed into the crucible.

2. As shown in Figure 3.6, a wire mesh was used to minimize thermocouple movement in the crucible. Two thermocouples were placed into the crucible – one at the center using the holder as a guide and a second thermocouple at the outer diameter of the crucible.
3. The crucible was suspended into position within the furnace.
4. The furnace was set to 375°C with a heating rate of 10°C/min.
5. Temperature measurements were collected at a rate of 1 Hz.

This experiment was repeated for the quartz crucible and each experiment was performed three times for both crucibles.

3.2.2 Analysis of Convective Heat Transfer

There were three modes of heat transfer within the thermal degradation system: conduction, convection, and radiation. Conduction occurs within materials subjected to temperature gradients. Convective heat transfer occurs between solids and fluids at different temperatures. Non-contact radiation heat exchange can occur when two bodies at different temperatures are in line-of-sight of each other.

Newton's Law of Cooling is often used to describe convective heat transfer:

$$Q_{conv} = hA(T_{surr} - T_s). \tag{3.1}$$

Q_{conv} is the convective heat transferred between the center of the sample and the fluid, h is the convective heat transfer coefficient, A is the surface area of the sample being heated, T_{surr} is the temperature of the surroundings, and T_s is the temperature of the material. During the heating cycle, T_{surr} is the temperature of the furnace and during the cooling cycle it is the temperature of the environment surrounding the sample. A requirement of Newton's Law is that the convective heat transfer coefficient remains constant, i.e. the heat flow per unit area is proportional to the

temperature difference between the sample and the surrounding fluid. The heat transfer coefficient has thus been assumed to be constant in this analysis. The thermophysical properties of the materials were also assumed to be constant.

The total thermal energy E_T stored in a sample at a given temperature can be defined as

$$E_T = mc_p T_s \tag{3.2}$$

where m is the mass of the sample, c_p is the specific heat capacity of the sample, and T_s is the temperature of the sample. Differentiating the total thermal energy with respect to time yields

$$\frac{dE_T}{dt} = mc_p \frac{dT_s}{dt} \tag{3.3}$$

which can be set equal to Equation (3.1) to obtain

$$-mc_p \frac{dT_s}{dt} = hA\left(T_{surr} - T_s\right) \tag{3.4}$$

Rearranging Equation (3.4) so that it can easily be integrated over temperature and time gives

$$\int_{T_i}^{T_s} \frac{dT_s}{\left(T_{surr} - T_s\right)} = \frac{-hA}{mc_p} \int_0^t dt \tag{3.5}$$

where the left hand side is integrated from initial temperature, T_i, to final sample temperature, T_s; and the right hand side is integrated from 0 to time, t. T_s is the dependent variable. Integration of both sides yields

$$\ln\left(T_{surr} - T_s\right)\Big|_{T_i}^{T_s} = \frac{-hA}{mc_p} t\Big|_0^t \tag{3.6}$$

Substituting in the integration limits gives

$$\ln\left(T_{surr} - T_s\right) - \ln\left(T_{surr} - T_i\right) = \frac{-hAt}{mc_p} \tag{3.7}$$

Solving for the final sample temperature yields

$$T_s = T_{surr} - (T_{surr} - T_i)\exp\left(\frac{-hAt}{mc_p}\right) \tag{3.8}$$

Taking the reciprocal of the coefficient of *t* yields the thermal time constant τ:

$$\tau = \frac{mc_p}{hA} \tag{3.9}$$

Rewriting equation 3.8 with τ yields

$$T_s = T_{surr} - (T_{surr} - T_i)\exp(-\pi t) \tag{3.10}$$

The thermal time constant describes the amount of time for the sample to reach 37% of its final temperature. Three times the thermal time constant will indicate approximately when the sample is approaching or has essentially reached its steady state temperature. According to the literature, the heat transfer coefficient for aluminum under natural convection in air ranges from 5 to 35 $W/m^2 \cdot K$ [30-32]. These values can be used to estimate the thermal time constant of the system. The thermal time constant was then used to calculate convective heat transfer coefficients for the quartz and steel crucibles, respectively.

3.2.3 Analysis of Radiative Heat Transfer

In this section, radiation is considered to be the only heat transfer mechanism. The thermophysical properties of the materials were again assumed to be constant.

The Stefan-Boltzmann Law is the governing relationship for heat transfer by radiation and is given by

$$Q_{s\rightarrow surr} = A\varepsilon F_{12}\sigma\left(T_s^4 - T_{surr}^4\right) \tag{3.13}$$

Where $Q_{s\rightarrow surr}$ is the radiative heat exchange between the sample and the surroundings, *A* is the radiating area, ε is the emissivity, F_{12} is the view factor, σ is the Stefan-Boltzmann constant, T_s is the temperature of the sample, and T_{surr} is the temperature of the surroundings. As in the previous

section, T_{surr} is the temperature of the surrounding environment. The crucible was assumed to be in complete line-of-sight of its surroundings thus allowing one to assume a geometric view factor of one. Equation (3.13) can be set equal to the right hand side of equation (3.3):

$$-mc_p \frac{dT_s}{dt} = A\varepsilon\sigma\left(T_s^4 - T_{surr}^4\right) \tag{3.14}$$

If T_s is very large compared to T_{surr}, then it can be assumed that T_{surr}^4 is insignificant. To integrate this equation over time and temperature, it is rearranged to yield

$$\int_{T_i}^{T_s} \frac{dT_s}{T_s^4} = \frac{A\varepsilon\sigma}{-mc_p} \int_0^t dt \tag{3.15}$$

where the left hand side is integrated from initial sample temperature to final sample temperature and the right hand side is integrated from zero to time, *t*. Equation (3.15) is integrated over time and temperature and rearranged to yield

$$\frac{-1}{3T_s^3}\Bigg|_{T_i}^{T_s} = \frac{A\varepsilon\sigma}{-mc_p} t\Big|_0^t \tag{3.16}$$

Substituting for the integration limits yields

$$\frac{-1}{3T_s^3} + \frac{1}{3T_i^3} = \frac{A\varepsilon\sigma t}{-mc_p} \tag{3.17}$$

From the previous equation it is possible to obtain the final temperature of the sample

$$T_s = \left(\frac{1}{3\left(\frac{A\varepsilon\sigma t}{mc_p} + \frac{1}{3T_i^3} \right)} \right)^{1/3} \tag{3.18}$$

3.3 Experimental Arrangement to Evaluate Mass Measurements of System

The mass measurements of the microbalance were evaluated with one milliliter of Aeroshell 560 Turbine Oil in the quartz crucible. The purpose of this experiment was to determine the repeatability of the mass measurements with the microbalance. The experimental protocol for the mass measurements was carried out with the following steps:

1. One milliliter (1 g) of Aeroshell 560 Turbine Oil was placed into the quartz crucible.
2. The crucible was suspended into position within the furnace.
3. The furnace was set to 375°C with a heating rate of 10°C/min.
4. Mass measurements were collected at a rate of 1 Hz.

The experiment was repeated 5 times. The mass change rate was calculated by taking the difference of the mass over the change in time.

3.4 Experimental Arrangement to Thermally Degrade Jet Engine Oil

The capabilities of the system as a whole were evaluated with one milliliter of Mobil Jet Oil II. The experimental protocol to thermally degrade the Mobil Jet Oil II was carried out with the following steps:

1. One milliliter (1 g) of Mobil Jet Oil II was placed into the quartz crucible.
2. The thermocouple was centered without touching the bottom of the crucible.
3. The crucible was suspended into position within the furnace.
4. The bell jar was placed over the balance – furnace assembly.
5. The door of the fume hood was secured.
6. The furnace was set to 375°C with a heating rate of 10°C/min.
7. Temperature and mass measurements were each collected at a rate of 1 Hz.
8. Once the set point was reached, the oil sample was held isothermally for one hour.

Measurements from commercial CO and CO_2 sensors were also obtained at 5 minute intervals and FTIR scans were taken every 2 minutes. Figure 3.7 shows a schematic of the experimental set-up. For this study, a TGS 5042 CO sensor made by Figaro (Arlington Heights, IL) and an EE80-2CT2/TO4 CO_2 sensor made by AirTest (Delta, BC) were used [33]. The TGS 5042 is an electrochemical sensor that utilizes amperometry to calculate the CO concentration by means of a working electrode and a counter electrode. Specific anions dissolved in an electrolyte oxidize the CO present at the working electrode generating a current proportional to the CO concentration. The sensor has an automatic calibration procedure to compensate for the aging of the infrared source and dust contamination. The EE80 utilizes non-dispersive infrared (NDIR) technology. The sensor has two single wavelength infrared sources. The first infrared source continuously monitors the sample chamber whereas the second infrared source is used as a reference signal for calibration. The sensor calculates the amount of CO_2 present based on the absorbed energy of the infrared beam after it has traveled through the sensors sample chamber. The FTIR was a Perkin-Elmer Spectrum GX Fourier Transform Infrared Spectrometer and is described in detail by Haney et al [34]. The sensors were housed in a sensor chamber separate from the bell jar. A line was run from the six-way cross below the base plate to the sensor chamber and from the sensor chamber to the FTIR. A vacuum pump connected to the FTIR pulled air through the whole system at a rate of 11,600 sccm into the building exhaust.

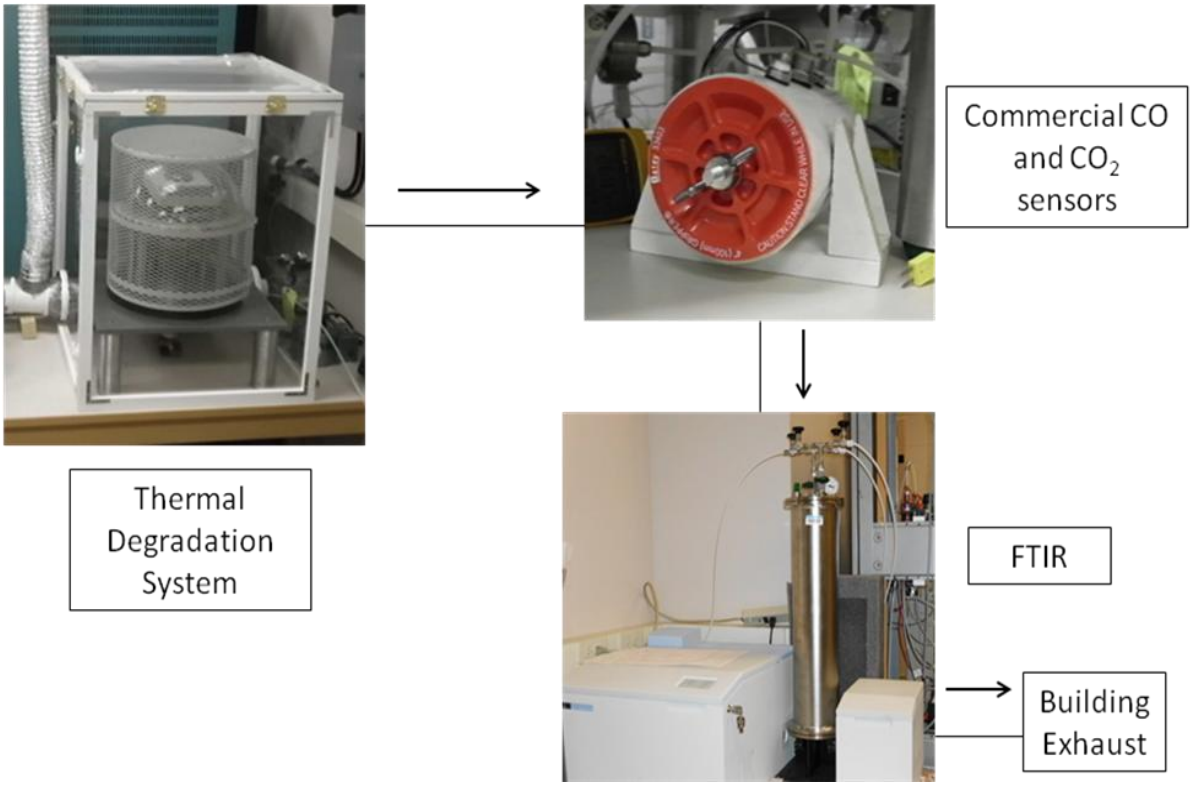

Figure 3.7: Schematic of experimental set-up for oil degradation.

4. Results and Discussion

4.1 Heat Transfer Analysis

4.1.1 Analysis of Temperature Measurements

The heating and cooling temperature profiles of an aluminum slug, a stainless steel crucible, and a quartz crucible were recorded for a range of furnace temperatures: 300, 350, 400, 450, and 500°C. The sample temperature change was plotted as a function of time and the plots are shown in Figures 4.1, 4.2, and 4.3, respectively.

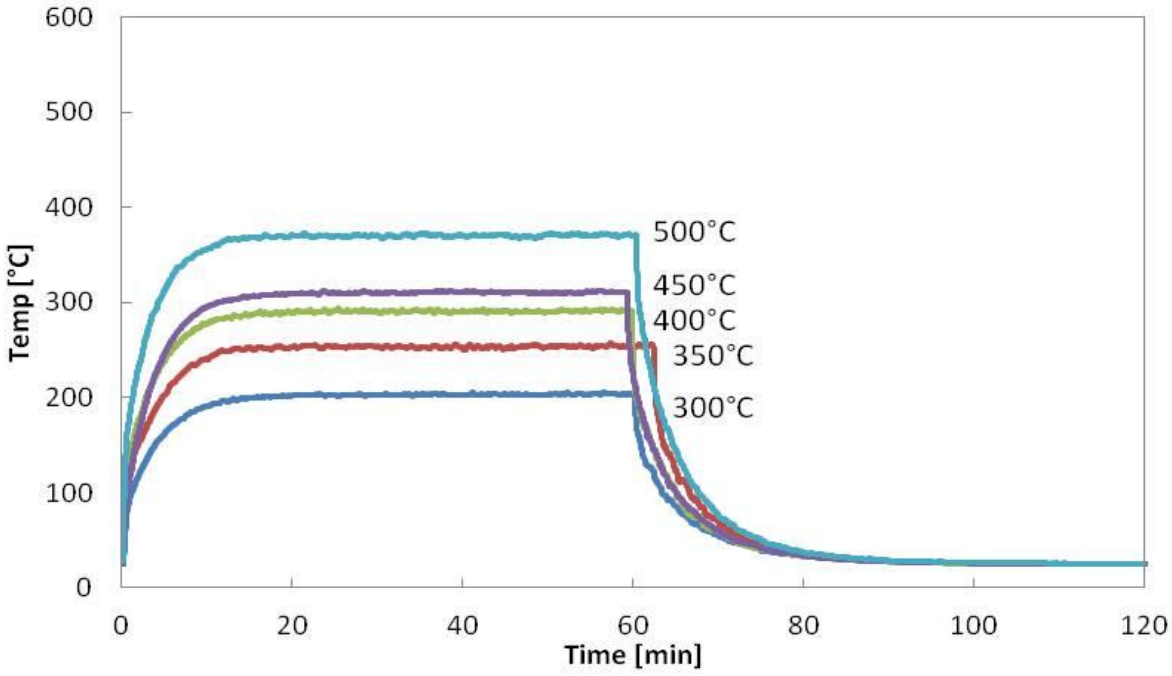

Figure 4.1: Temperature profiles for aluminum slug at the indicated furnace set points.

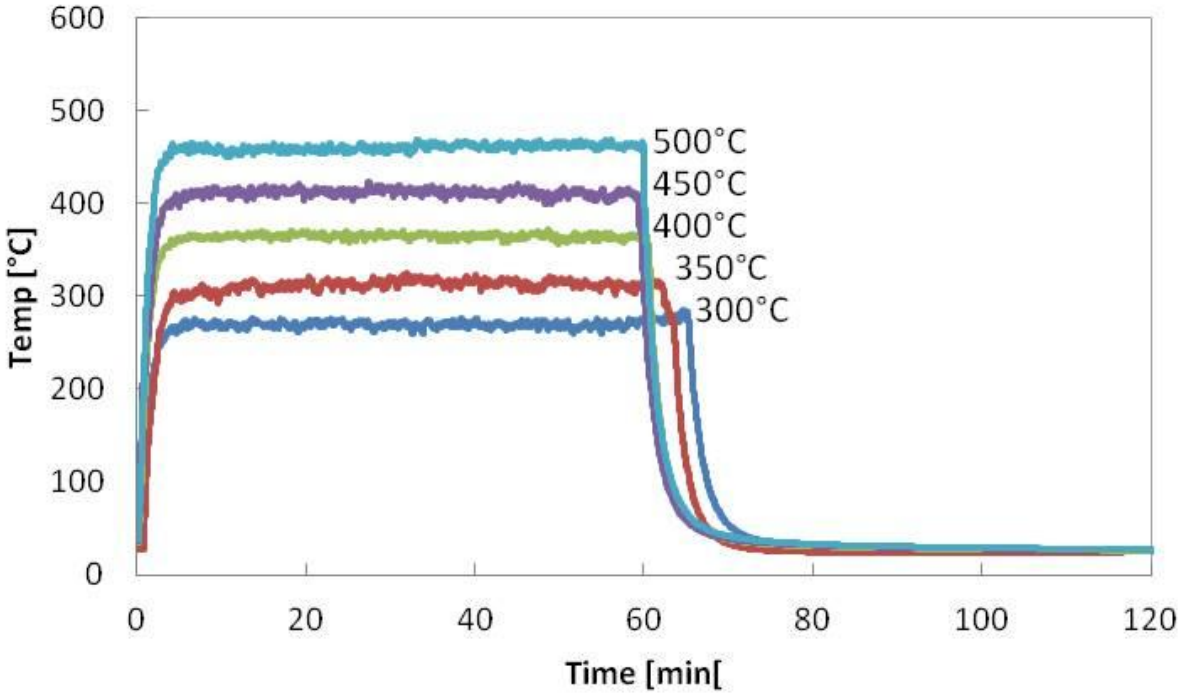

Figure 4.2: Temperature profiles for steel crucible at the indicated furnace set points.

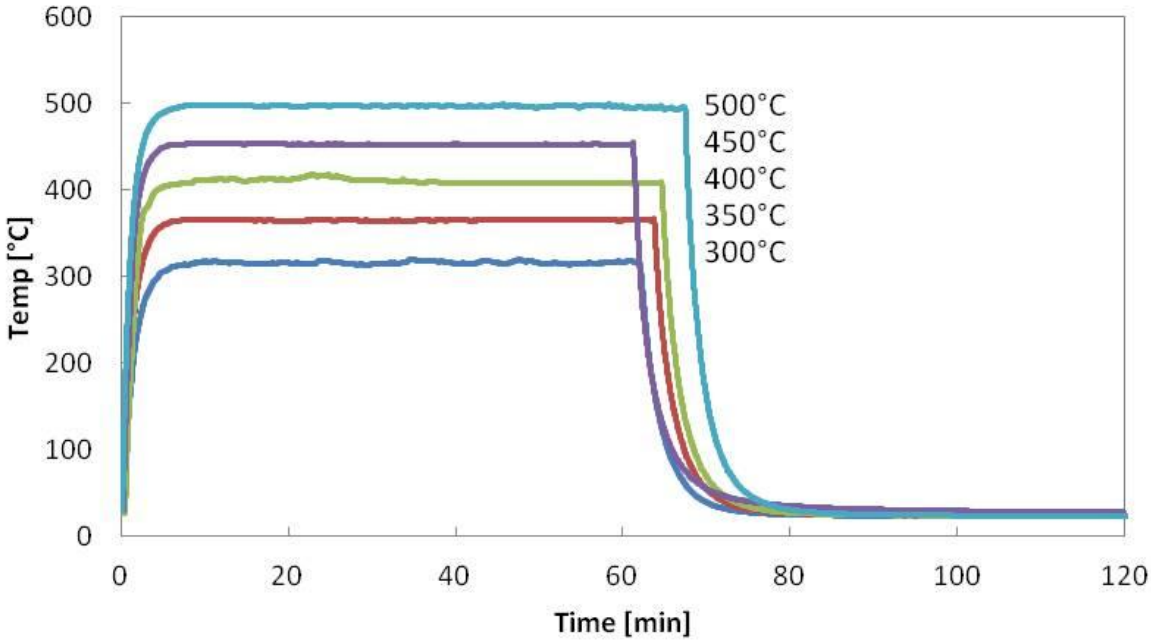

Figure 4.3: Temperature profiles for quartz crucible at the indicated furnace set points.

Even though all three samples were evaluated with the same furnace set points, each sample reached different final steady state temperatures. The quartz crucible is the only sample whose steady state temperature was at or slightly above the furnace temperature. Quartz absorbs certain infrared wavelengths emitted by radiative heat. The wavelengths absorbed are between 2.6 and 2.9, and above 3.6 μm [35, 36]. If these wavelengths are present in the furnace when heating the quartz crucible may be absorbing them, which could potentially cause the quartz crucible to gain additional heat from the absorbed wavelengths. The average temperature difference between the furnace set point and the steady state temperature of the aluminum slug was 110 ± 8°C. The average temperature difference between the furnace set point and the steady state temperature of the steel crucible was 50 ± 5°C. The steady state temperature of the aluminum slug and the steel crucible never equals the furnace set point because of heat losses due to convection and radiation. The aluminum slug and the steel crucible lose heat to the surroundings at different rates due differences in their respective geometries. The aluminum slug, as shown in Figure 3.2, was a rectangle with a hole in the center for the thermocouple. The aluminum slug heats from the outside and conducts heat inward to the thermocouple location. This process is slow and possibly contributes to the large difference between the steady state temperature of the aluminum slug and the furnace set point. Additionally, the rate of temperature increase of the aluminum slug is also affected causing it to take longer to reach its steady state temperature. The steel crucible, as shown in Figure 3.2, is a hollow, thin-walled cylinder with one end closed. The sides of the crucible heat up first because they are in the line-of-sight of the heater. Then heat is transferred to the bottom of the crucible.

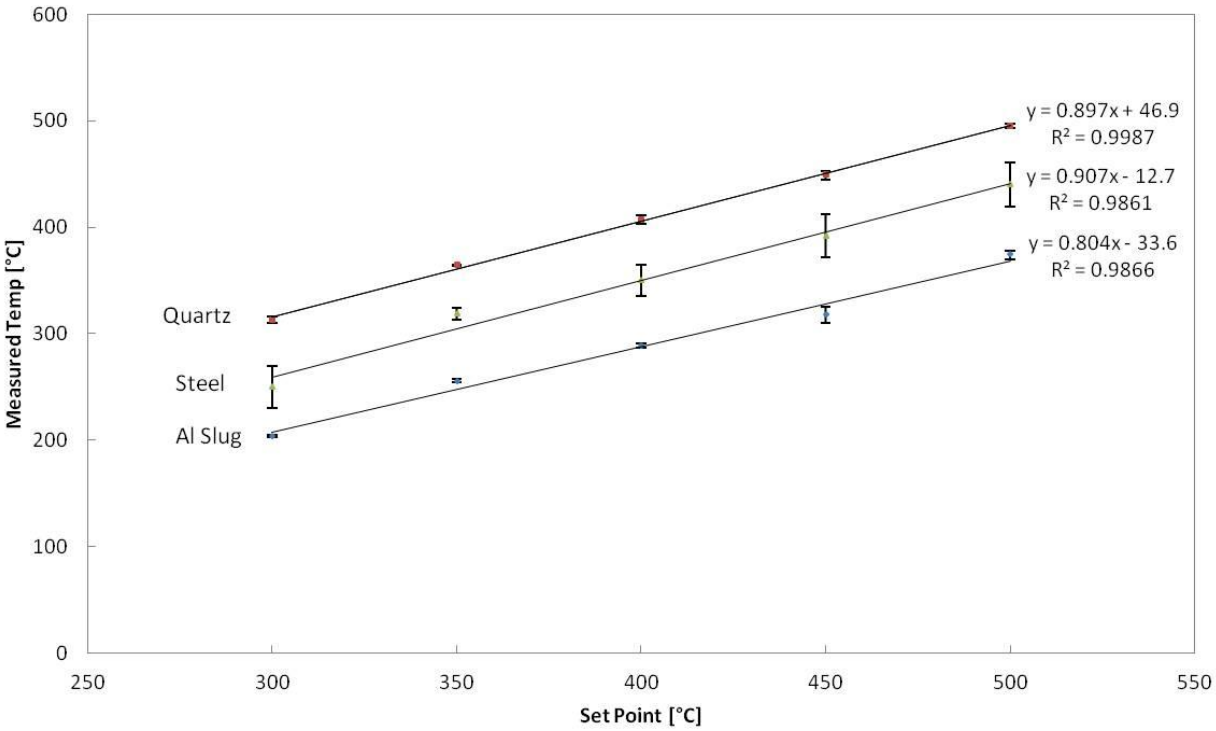

Figure 4.4: Calibration curve for the crucibles.

The calibration curve for the crucibles is shown in Figure 4.4 and the curve for the aluminum slug is also shown for comparison. The steady state temperature of each of the samples is plotted with the furnace set point. For either crucible, the equations obtained from the linear curve fit can be used to predict the final temperature of the empty crucible, which can provide an approximation for the final temperature of the oil in the crucible.

The calibration curve shows that the quartz crucible had the highest steady state temperature; the steel crucible had the second highest steady state temperature, and the aluminum slug had the lowest steady state temperature. The steady state temperatures of the steel crucible and the aluminum slug are lower than the furnace set point due to heat losses to the surroundings. The steel crucible and the aluminum slug also have reflective surfaces that reflect heat away causing the thermocouple to measure lower temperatures. As mentioned previously,

the quartz crucible absorbs certain wavelengths of radiative heat, which may cause it to have a higher temperature than its surroundings. In this case, the quartz crucible may potentially radiate heat to the surrounding air and maintain a temperature at or slightly above the furnace set point. Additionally, the quartz had the lowest uncertainty and the steel crucible had the largest uncertainty in temperature measurements. According to these results, the quartz crucible is the best candidate for oil thermal degradation experiments because of its low uncertainty.

4.1.2 Convection

Convection was initially considered to be the only heat transfer mechanism occurring in the system. Convective heat transfer coefficients were estimated for the aluminum slug, the steel crucible, and the quartz crucible. The equations of the exponential curve fits and the time constants calculated from these equations for the aluminum slug, the steel crucible, and the quartz crucible during the heating cycle are presented in Tables 4.1, 4.2, and 4.3, respectively. According to Table 4.1, the time constants calculated from the exponential curve fits for the aluminum slug during the heating cycle range from approximately 200 to 250 s. The corresponding heat transfer coefficients for these time constants are 20 to 25 $W/m^2 \cdot K$ where the lower heat transfer coefficient is associated with the higher time constant. The time constant decreases as the furnace set point increases. A smaller time constant indicates that the sample is responding faster to its environment. This is a possible indication of radiation contributing to heat transfer between the aluminum slug and the surroundings.

According to Table 4.2, the time constants calculated from the exponential curve fits for the steel crucible during the heating cycle range from approximately 60 to 90 s. The corresponding heat transfer coefficients for these time constants are 20 to 30 $W/m^2 \cdot K$. Even though the aluminum slug and the steel crucible have similar heat transfer coefficients the time

constants are different because they are dependent on material properties, such as specific heat capacity. Aluminum has a specific heat capacity of 896 J/kg·K and steel has a specific heat capacity of 500 J/Kg·K. Specific heat capacity describes the amount of energy required to change one unit of mass of a substance by one unit of temperature. The lower specific heat capacity a substance has the less energy that is required to raise its temperature. In this case, the steel has a lower specific heat capacity and thus requires less energy to raise its temperature, in turn requiring less time to reach 37% of its final temperature. The mass and the surface area also contribute to the time constant. A larger mass increases the time constant while larger surface areas decrease the time constant.

Furnace Set Point [°C]	Equation	R^2	Time Constant [s]
300	$T_s = 149e^{-0.00404t}$	0.987	248
350	$T_s = 186e^{-0.00414t}$	0.991	242
400	$T_s = 211e^{-0.00444t}$	0.99	225
450	$T_s = 305e^{-0.00509t}$	0.999	196
500	$T_s = 266e^{-0.00490t}$	0.991	204

Table 4.1: The equations of the exponential curves fit to the experimental temperature curves of the aluminum slug during the heating cycle and the calculated time constants.

Furnace Set Point [°C]	Equation	R^2	Time Constant [s]
300	$T_s = 277e^{-0.0117t}$	0.988	85
350	$T_s = 418e^{-0.0109t}$	0.984	92
400	$T_s = 383e^{-0.0146t}$	0.987	68
450	$T_s = 395e^{-0.0124t}$	0.971	81
500	$T_s = 563e^{-0.0170t}$	0.988	59

Table 4.2: The equations of the exponential curves fit to the experimental temperature curves of the steel crucible during the heating cycle and the calculated time constants.

Furnace Set Point [°C]	Equation	R^2	Time Constant [s]
300	$T_s = 296e^{-0.0100t}$	0.993	100
350	$T_s = 387e^{-0.0129t}$	0.999	78
400	$T_s = 299e^{-0.00891t}$	0.903	112
450	$T_s = 484e^{-0.0147t}$	0.995	68
500	$T_s = 385e^{-0.0121t}$	0.986	83

Table 4.3: The equations of the exponential curves fit to the experimental temperature curves of the quartz crucible during the heating cycle and the calculated time constants.

According to Table 4.3, the time constants calculated from the exponential curve fits for the quartz crucible during the heating cycle range from approximately 70 to 110 s. The corresponding convective heat transfer coefficients for these time constants are 30 to 45 $W/m^2 \cdot K$. Also the convective heat transfer coefficient values calculated for quartz are a little higher than those calculated for the aluminum slug and the steel crucible. This indicates that radiation is likely contributing to heat transfer for the quartz. This is plausible considering that quartz is nearly invisible to radiation as mentioned previously and so it is reasonable that radiation would be more apparent in the quartz crucible calculations than the aluminum slug or the steel crucible.

The equations of the exponential curve fits and the time constants calculated from these equations for the aluminum slug, the steel crucible, and the quartz crucible during the cooling cycle are presented in Tables 4.4, 4.5, and 4.6, respectively. According to Table 4.4, the time constants calculated from the exponential curve fits for the aluminum slug during the cooling cycle range from approximately 330 to 500 s. The corresponding convective heat transfer coefficients for these time constants are 10 to 15 $W/m^2 \cdot K$.

Furnace Set Point [°C]	Equation	R^2	Time Constant [s]
300	$T_s = 179e^{-0.00200t}$	0.932	500
350	$T_s = 230e^{-0.00214t}$	0.904	467
400	$T_s = 265e^{-0.00219t}$	0.911	457
450	$T_s = 297e^{-0.00201t}$	0.961	498
500	$T_s = 344e^{-0.00223t}$	0.927	448

Table 4.4: The equations of the exponential curves fit to the experimental temperature curves of the aluminum slug during the cooling cycle and the calculated time constants.

Furnace Set Point [°C]	Equation	R^2	Time Constant [s]
300	$T_s = 236e^{-0.00792t}$	0.995	126
350	$T_s = 407e^{-0.00816t}$	0.978	123
400	$T_s = 336e^{-0.00869t}$	0.995	115
450	$T_s = 441e^{-0.00796t}$	0.995	126
500	$T_s = 392e^{-0.00806t}$	0.993	124

Table 4.5: The equations of the exponential curves fit to the experimental temperature curves of the steel crucible during the cooling cycle and the calculated time constants.

Furnace Set Point [°C]	Equation	R^2	Time Constant [s]
300	$T_s = 276e^{-0.00620t}$	0.999	161
350	$T_s = 319e^{-0.00643t}$	0.998	156
400	$T_s = 347e^{-0.00638t}$	0.996	157
450	$T_s = 380e^{-0.00636t}$	0.990	157
500	$T_s = 425e^{-0.00706t}$	0.9957	142

Table 4.6: The equations of the exponential curves fit to the experimental temperature curves of the quartz crucible during the cooling cycle and the calculated time constants.

According to Table 4.5, the time constant calculated from the exponential curve fits for the steel crucible during the cooling cycle range from approximately 115 to 125 s. The

corresponding convective heat transfer coefficient for the time constants is 15 $W/m^2 \cdot K$. According to Table 4.6, the time constants calculated from the exponential curve fits for the quartz crucible during the cooling cycle range from approximately 140 to 160 s. The corresponding convective heat transfer coefficients for these time constants are 15 to 20 $W/m^2 \cdot K$. During the cooling cycle, the samples did not show much variation in the thermal time constants. Quartz exhibited the largest calculated heat transfer coefficient. According to the previous section, quartz loses very little if any heat to its surroundings during heating. The convective heat transfer coefficient is proportional to the heat flux and the temperature difference between the sample and its surroundings. The quartz crucible has a larger convective heat transfer coefficient because it is not losing as much heat per unit area as the steel crucible or the aluminum slug. The heat transfer coefficients are much larger on heating than the heat transfer coefficients calculated on cooling, because during heating there are multiple heat transfer mechanisms occurring, i.e. convection and radiation. On cooling, convection appears to be the dominant mode of heat transfer.

The convective heat transfer coefficients and time constants calculated for the aluminum slug, the steel crucible, and the quartz crucible at each of the furnace set points were consistent. This allowed averages to be calculated for the values of the heat transfer coefficients and the time constants at each of the furnace set points. The results of these calculations for both the heating cycle and the cooling cycle with standard errors are presented in Tables 4.7 and 4.8, respectively.

	Average Time Constants [s]	Heat Transfer Coefficient [W/m^2·K]
Al Slug	223 ± 10	22 ± 1.0
Steel	77 ± 6	22 ± 2.0
Quartz	88 ± 8	34 ± 3.0

Table 4.7: Summary of the time constants calculated from the exponential curve fits and their corresponding heat transfer coefficients for the heating cycle.

	Average Time Constants [s]	Heat Transfer Coefficient [W/m^2·K]
Al Slug	474 ± 11	10 ± 0.5
Steel	123 ± 2	14 ± 0.5
Quartz	155 ± 3	19 ± 0.5

Table 4.8: Summary of the time constants calculated from the exponential curve fits and their corresponding heat transfer coefficients for the cooling cycle.

4.1.3 Radiation

The effects of radiation on the heat transfer of the aluminum slug were also considered. According to the literature, the emissivity of aluminum is reported to be approximately 0.5 [37-39]. Equation 3.18 from section 3.2.3 was used to predict the temperatures of the aluminum slug at a furnace set point of 500°C as if radiation was the only heat transfer mechanism occurring. This set point was chosen because it was assumed that radiation was more likely to be apparent at the higher temperatures. Only the cooling cycle was evaluated. The results were compared with the experimentally obtained curve and are shown in Figure 4.5.

The theoretically predicted curve matches the experimentally obtained curve briefly at the very beginning of the cooling process, but it seems that convection quickly begins to dominate. It may be possible that at furnace set points above 500°C radiation becomes even more important. Because the contribution from radiation appears to be so small similar analyses were not carried out for the steel or quartz crucibles.

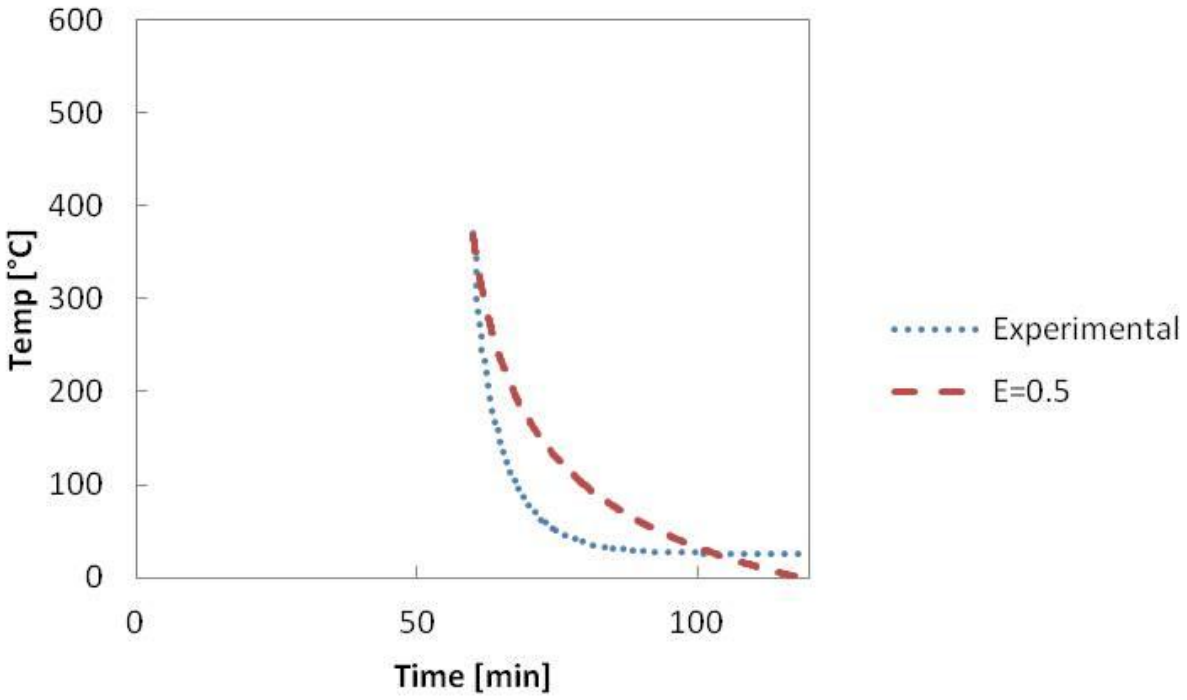

Figure 4.5: Comparison of the predicted temperature curve due to radiation with the experimentally determined curve.

The power lost due to convection and due to radiation was calculated to provide a quantitative perspective of their relative contributions to the overall heat transfer of the system. Power lost due to convection was calculated using $Q_{conv} = hA(T_{surr} - T_s)$. Power lost due to radiation was calculated using $Q_{s\to surr} = A\varepsilon F_{12}\sigma(T_s^4 - T_{surr}^4)$. The results are shown in Table 4.9 for the aluminum slug and the steel crucible, respectively, along with the percentage of heat lost due to convection for each of the steady state temperatures obtained from heating the samples to various furnace set points. Overall, approximately 20% of the power losses can be attributed to radiation. As the steady state temperature increases radiation becomes more dominant.

Al Slug				Steel			
Steady State Temperature [°C]	**Q_{conv} [W]**	**Q_{rad} [W]**	**% power loss due to convection**	**Steady State Temperature [°C]**	**Q_{conv} [W]**	**Q_{rad} [W]**	**% power loss due to convection**
204	3.49	0.231	93.8	250	6.96	0.558	92.6
256	3.43	0.390	89.8	318.5	4.39	0.627	87.5
289	4.03	0.677	85.6	350	6.96	1.41	83.2
318	4.81	1.12	81.1	392	8.08	2.31	77.7
374	4.58	1.56	74.6	440	8.36	3.33	71.5
Average			85.0	Average			82.5

Table 4.9: Power lost due to convection at each of the steady state temperatures.

4.1.4 Temperature Gradients in Crucibles

The temperature gradients in the steel crucible and the quartz crucible with Aeroshell 560 Turbine Oil were measured by placing a thermocouple in the outer diameter of the crucible and another in the center of the crucible. The crucibles were heated to 375°C at a heating rate of 10°C/min. Table 4.10 shows the results of the temperature measurements from the center and outer diameter of the steel crucible. The overall percent difference between the center temperature measurements and the outer diameter temperature measurements range from 0.19% to 0.54%. Table 4.11 shows the results of the temperature measurements from the center and outer diameter of the quartz crucible. The overall percent differences between the center and the outer diameter range from 0.45% to 0.64%.

	Run 1	**Run 2**	**Run 3**
Ave. Steady State Temp. [K] - Center	673 K	657 K	680 K
Ave. Steady State Temp. [K] - OD	672 K	658 K	681 K
Overall % difference	0.54K	0.19%	0.19%

Table 4.10: Steady state temperatures for the center and outer diameter (OD) of the steel crucible with the overall percent differences.

	Run 1	Run 2	Run 3
Ave. Steady State Temp. [K] – Center	659 K	681 K	693 K
Ave. Steady State Temp. [K] – OD	654 K	677 K	688 K
Overall % difference	0.64%	0.45%	0.56%

Table 4.11: Steady state temperatures for the center and OD of the quartz crucible with the overall percent differences.

The differences between the center measurements and the outer diameter measurements of the steel crucible was very small, approximately no more than 2°C overall. This is within the error of the thermocouple measurements. The difference between the center measurements and the outer diameter measurements of the quartz crucible was approximately 5°C. This is larger than the error of the thermocouple measurements; however, the temperature gradient is small enough to assume uniform heating was occurring in the crucible. The combined average temperature of the steel crucible with the oil from the center and outer diameter measurements was 397 ± 4°C. The combined average temperature of the quartz crucible with the oil from the center and outer diameter measurements was 402 ± 6°C.

4.2 Mass Change Measurements

The sensitivity of the microbalance to changes in mass was evaluated by heating one milliliter of Aeroshell 560 Turbine Oil in the quartz crucible six times. The furnace set point was 375°C at a heating rate of 10°C/min. The mass change of the oil as a function of time is presented in Figure 4.6. There were variations in the starting mass for each of the runs due to operator error when using the pipette to measure out the amount of oil. Despite this variation, the oil begins to significantly lose mass at approximately 25 minutes into the experiment in each of the runs. Additionally, the final mass of the oil never reaches zero. This is confirmed by the solid black residue found in the bottom of the crucible after the experiment. Van Netten et al [2, 4] and

Crane et al [27] also found that a solid black residue, referred to as char, was left behind after heating jet engine oils. Figure 4.7 shows the mass change as a function of furnace temperature. The oil begins to significantly lose mass when the furnace reaches approximately 275°C. This is in agreement with the observations reported by Van Netten et al [2, 4].

The mass change rates of Aeroshell 560 Turbine Oil at a furnace set point of 375°C are shown in Figure 4.8. These plots confirm that significant mass change began to occur 25 minutes into the experiment. The peak mass change occurred at 40 minutes into the experiment during each of the runs even though the magnitude of the peak varied slightly for each of the runs. The average mass change rate at 40 minutes was found to be -0.0608 ± 0.0026 g/min. Also the mass change rate approaches zero as the mass of the oil becomes very small.

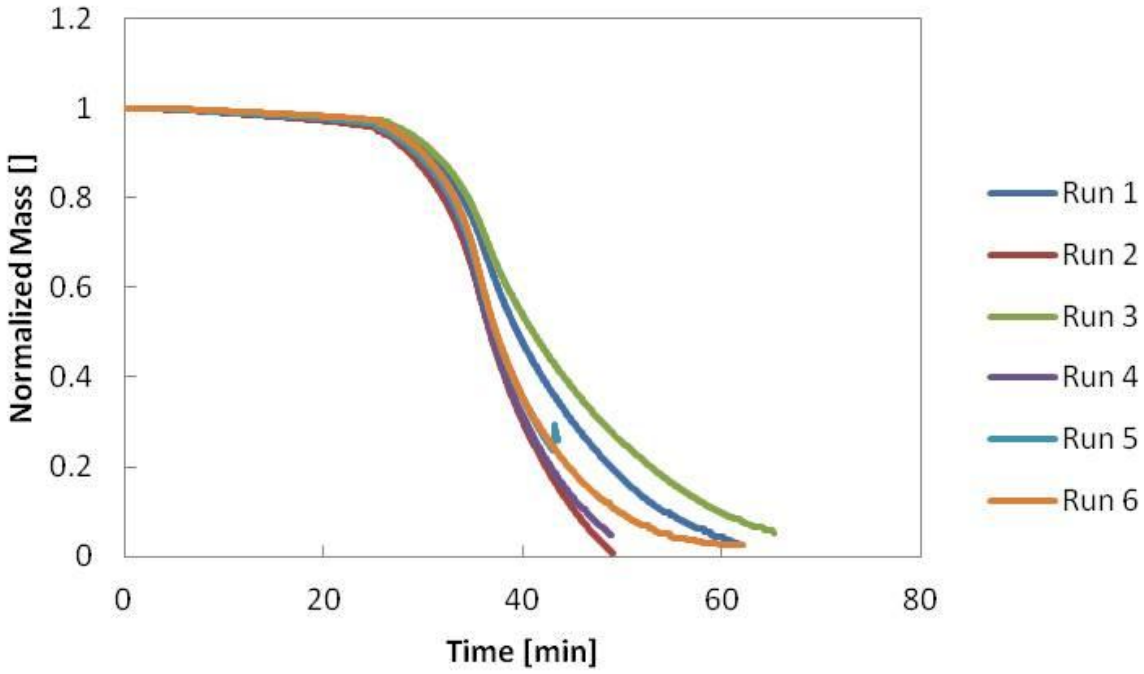

Figure 4.6: Mass change of Aeroshell 560 Turbine Oil for a furnace set point of 375°C.

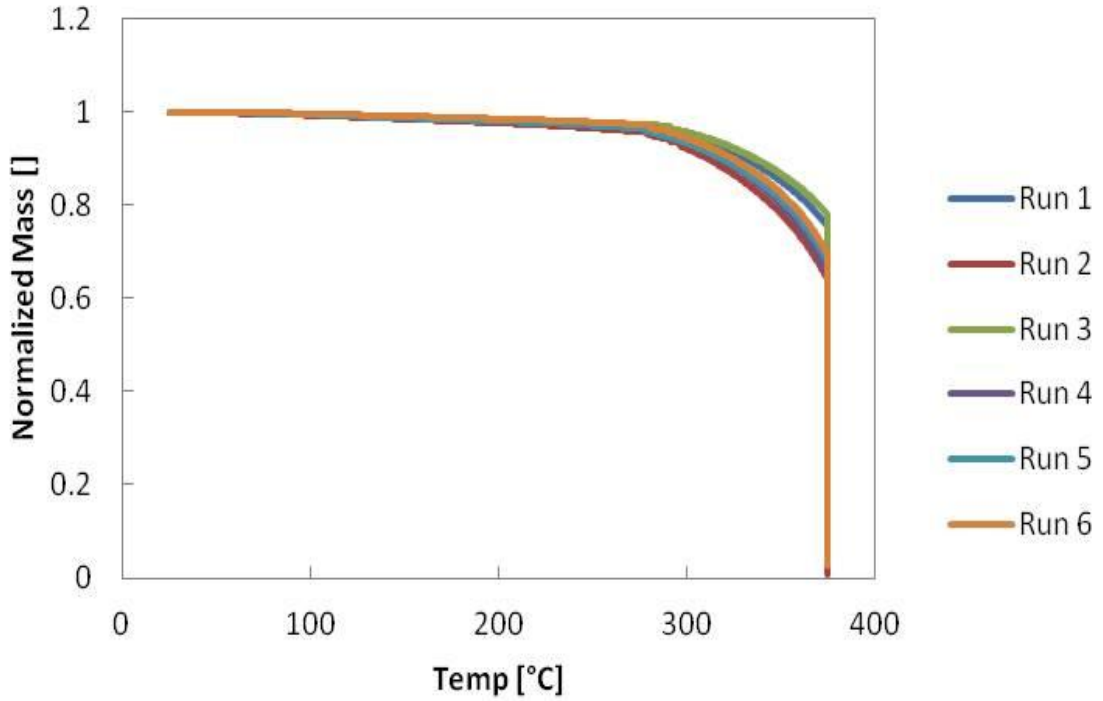

Figure 4.7: Mass change of Aeroshell 560 Turbine Oil as a function of furnace temperature for a set point of 375°C.

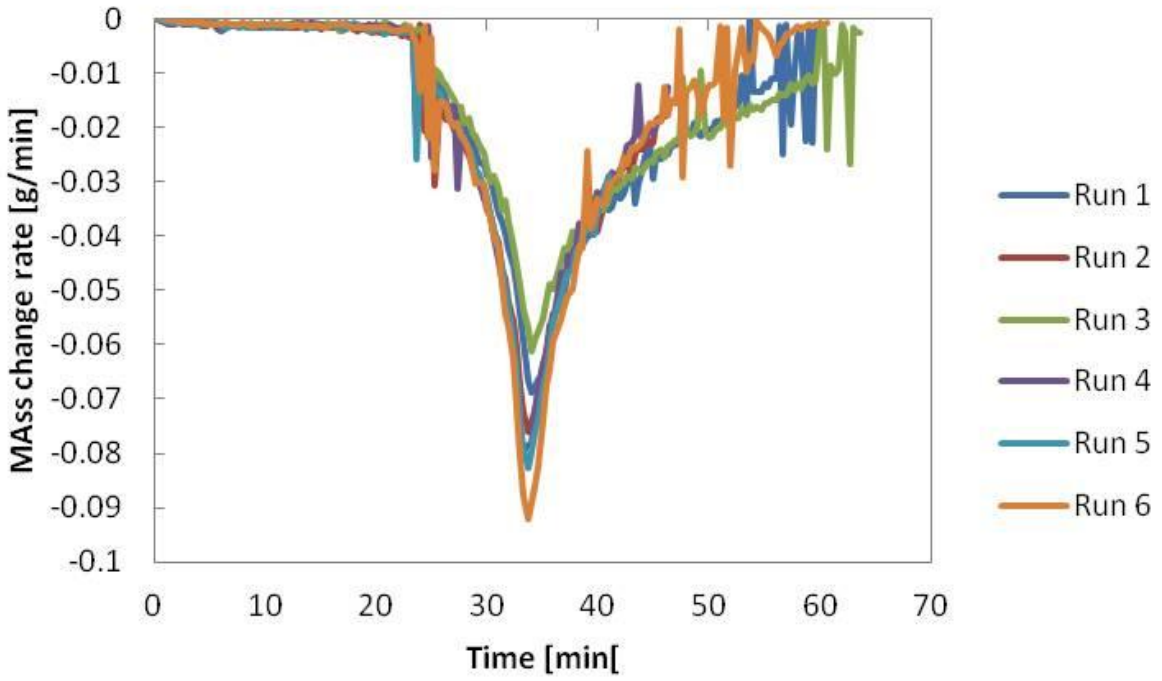

Figure 4.8: Mass change rates of Aeroshell 560 Turbine Oil with a furnace set point of 375°C.

4.3 Preliminary Results of Mobil Jet Oil II

The following sections discuss the results obtained from degrading 1 g of Mobil Jet Oil II. The furnace set point was 375°C with a heating rate of 10°C/min [33].

4.3.1 Mass Change and Temperature Measurements

Figure 4.9 shows the plot of mass versus time and temperature versus time for Mobil Jet Oil II. The oil begins to lose mass at approximately 190°C, 30 minutes into the experiment, which coincides with the time that white smoke was first observed. The oil achieves a steady state temperature of 225°C. At the end of the experiment, charred black material remained in the crucible. The mass of the crucible with the charred material was measured and the empty mass of the crucible was subtracted to yield a final mass of 0.0878 g of charred material, approximately

9% of the initial mass. The charred material is possibly due to high molecular weight products or polymers formed during degradation [19, 23].

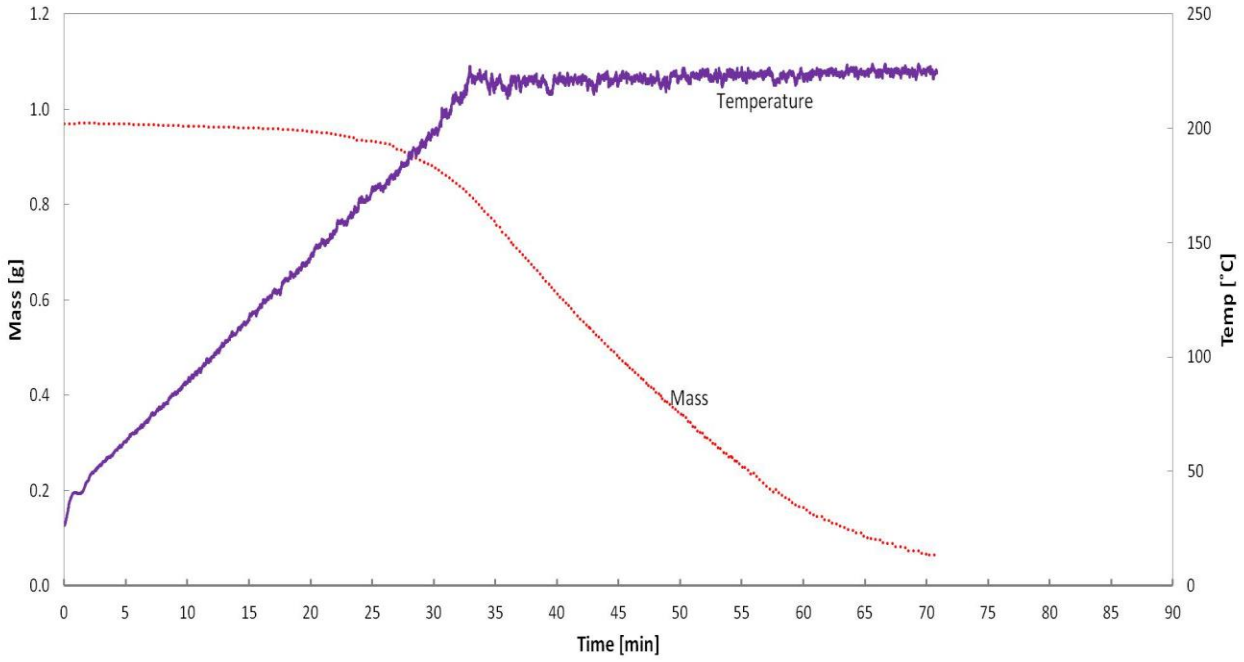

Figure 4.9: Plot of the oil mass (dashes) and temperature as functions of time.

4.3.2 Overall Appearance and Color Change

The oil was amber colored at room temperature before any degradation occurred. At the time that significant mass loss was noted and smoke was observed (approximately 30 minutes), the oil changed to a brown color. After approximately 40 minutes total had elapsed, the oil turned completely black and the bell jar filled with smoke, shown in Figure 4.11b. At this time the oil had reached its steady state temperature, 225°C. The mass of the oil at this time was roughly 0.6 g. The oil continued to lose mass indicating that degradation of the oil was still occurring. Figure 4.10a

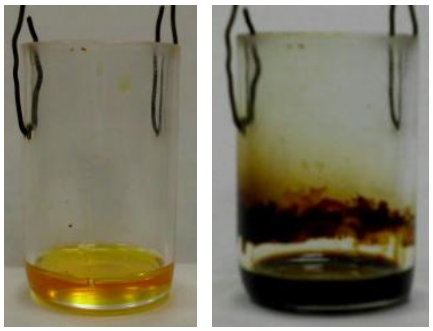

a) b)

Figure 4.10 a) Mobil Jet Oil II before thermal degradation, b) after thermal degradation.

shows Mobil Jet Oil II before thermal degradation and Figure 4.10b shows Mobil Jet Oil II after thermal degradation. The solid black residue or char was also observed by Van Netten et al [2, 4] and by Crane et al [27]. Those results are in agreement with Van Netten et al [2, 4].

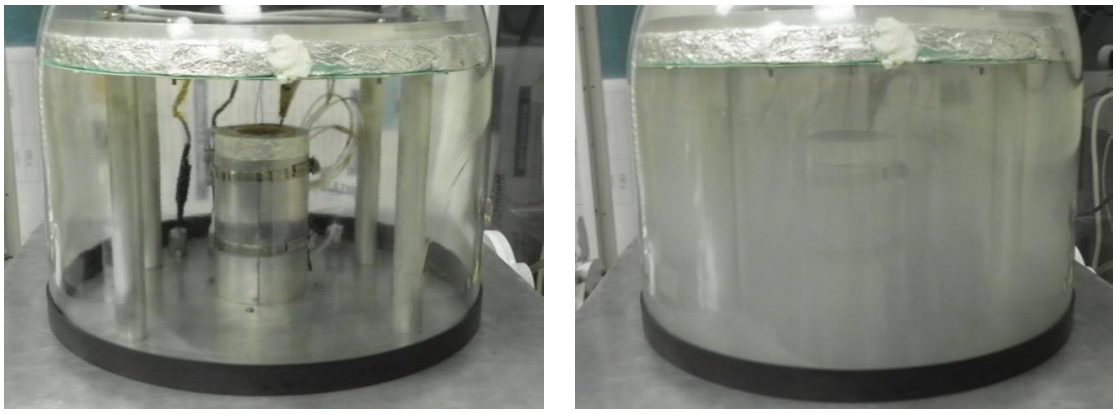

a) b)

Figure 4.11: a) Bell jar before degradation experiment, b) smoke-filled bell jar during degradation experiment.

4.3.3 Preliminary Sensor Results

Figures 4.12 and 4.13 show the change of CO and CO_2 concentration as a function of time along with the mass change. As mentioned previously, significant mass loss begins at approximately 30 minutes. Both sensors began detecting CO and CO_2 around that same time. The FTIR began detecting changes in the air samples about 5 minutes later. This time delay is due to the FTIR being connected downstream of the sensor chamber. Thus, the evolved gases will fill up the sensor chamber first and then the FTIR detection cell. The measured concentrations from the sensors and the FTIR appear to reach a peak when the mass of the oil is near zero and then begin to decrease again when degradation stops. The sensors and the FTIR were able to detect evolved gases from the degrading of Mobil Jet Oil II with fair correspondence to when smoke first appeared in the bell jar considering the time delays.

The sensors measured much larger concentrations of CO and CO_2 than was reported by Van Netten et al [2, 4]. The oil that was evaluated in this experiment is not the same brand that was analyzed by Van Netten and it is possible that the composition may be slightly different and could cause the amount of CO and CO_2 produced to be different. Also, this study evaluated a much larger sample of oil and it is possible that a larger sample of oil may produce more CO or CO_2.

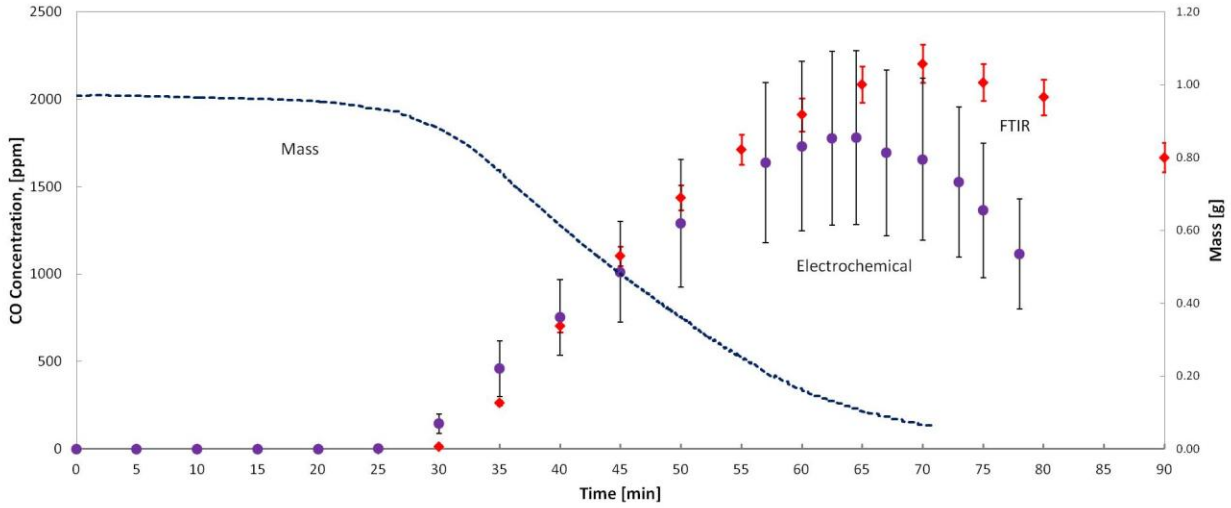

Figure 4.12: Plot of the change in CO concentration as a function of time as measured by the TGS5042 sensor (circles) and the FTIR (diamonds) and the mass (dashes) as a function of time.

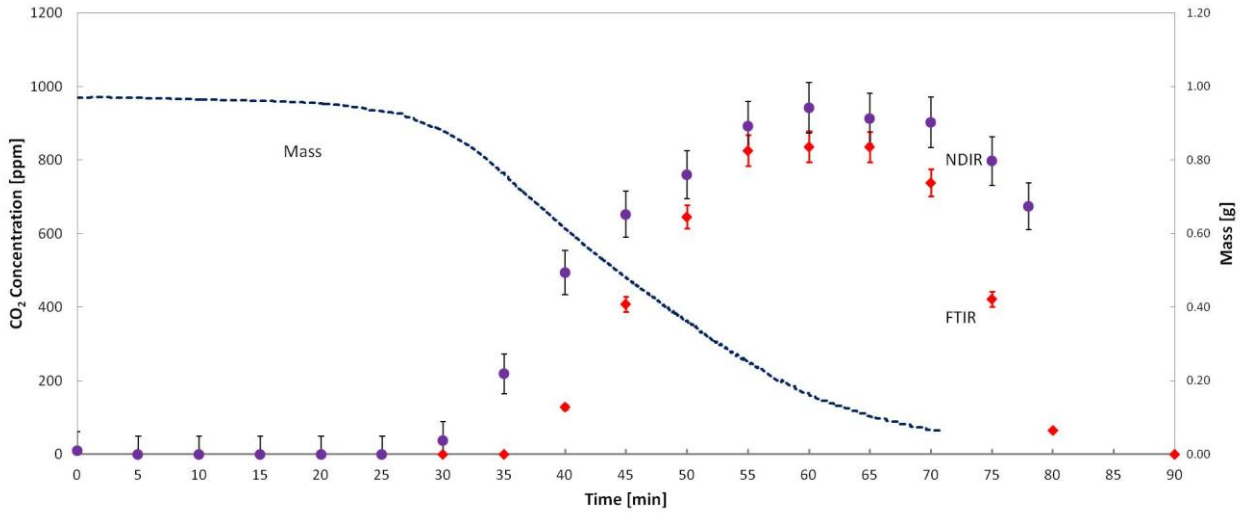

Figure 4.13: Plot of the CO_2 concentration as a function of time as measured by the EE80 (circles) and the FTIR (diamonds) and the mass (dashes) as a function of time.

5. Conclusions

A laboratory apparatus has been developed to study the thermal degradation behavior of jet engine oils by simultaneously measuring the temperature of the oil and its mass change. The system was able to investigate oils samples up to 2 g. Direct temperature measurements of the oil were also obtained without disrupting the microbalance measurements. The system was also successfully interfaced with a commercial sensor chamber and an FTIR.

Convection and radiation contribute to the heat transfer in the system. Convection is the most dominant mode of heat transfer though it is apparent that contribution by radiation increases with an increase in furnace set point. Calculating the energy transferred by radiation suggests that even at the highest furnace set point, the effect of radiation is still relatively small.

Heat transfer models were developed for convection and radiation. Thermal time constants were determined from the exponential curve fits of the data obtained from the heating and cooling cycles of the aluminum slug, the steel crucible, and the quartz crucible to describe how quickly the system responds to changes. Convective heat transfer coefficients were calculated from the experimentally determined thermal time constants for each of the samples. The temperature measurements of the aluminum slug and the steel crucible were not as well-behaved as the quartz crucible. It is recommended that the quartz crucible be used in future studies when studying the heat transfer of oil.

Mobil Jet Oil II behaved as expected during thermal degradation. The preliminary results of the thermal degradation behavior of this oil are consistent with results reported by other researchers

REFERENCES

1. Schrank, D., Lomax, T., Turner, S.,, *TTI's 2010 Urban Mobility Report*. 2010, Texas A&M University: College Station, TX. p. 60.

2. Van Netten, C., Leung, V.,, *Hydraulic Fluids and Jet Engine Oil: Pyrolysis and Aircraft Air Quality.* Archives of Environmental Health, 2001. **56**(2): p. 181-186.

3. Van Netten, C., *Multi-elemental Analysis of Jet Engine Lubricating Oils and Hydraulic Fluids and Their Implication in Aircraft Air Quality Incidents.* The Sci. of the Total Environ., 1999. **229**: p. 125-129.

4. Van Netten, C., Leung, V.,, *Comparison of the Constituents of Two Jet Lubricating Oils and Their Volatile Pyrolytic Degradation Products.* Applied Occupational and Environmental Hygiene, 2000. **15**(3): p. 277-283.

5. Murawski, J.T.L., Supplee, D.S.,, *An Attempt to Characterize the Frequency, Health Impact, and Operational Costs of Oil in the Cabin and Flight Deck Air Supply on U.S. Commercial Aircraft.* Journal of ASTM International, 2008. **5**(5): p. 1-15.

6. Winder, C., *Hazardous Chemicals on Jet Aircraft: Case Study - Jet Engine Oils and Aerotoxic Syndrome.* Current Topics in Toxicology, 2006. **3**: p. 65-88.

7. Hunt, E.H., Reid, D.H., Space, D.R., Tilton, F.E.,. *Commercial Airliner Environmental Control System: Engineering Aspects of Cabin Air Quality*. in *Aerospace Medical Association Meeting*. 1995. Anaheim, California.

8. Vincent, E.T., *The Theory and Design of Gas Turbines and Jet Engines*. 1950, PA: MacGraw-Hill Book Co., Inc.

9. Smith, C.W., *Aircraft Gas Turbines*. 1956, New York, New York: John Wiley and Sons, Inc.

10. Gunston, B., *The Development of Jet and Turbine Aero Engines*. 1995: Patrick Stevens Limited.

11. Mattingly, J.D., *Elements of Propulsion: Gas Turbines and Rockets*. 2006: American Institute of Aeronautics and Astronautics.

12. Hunt, E.H., Space, D.R.,. *The Airplane Cabin Environment*. in *Internatinal In-Flight Service Management Organization Conference*. 1994. Montreal, Canada.

13. National Research Council, D.o.L.a.E.S., Board on Environmental Studies and Toxicology, Committee on Air Quality in Passenger Cabins of Commercial Aircraft, *The Airliner Cabin Environment and the Health of Passengers and Crew*, ed. N.R.C. Report. 2002: National Academy Press.

14. Winder, C., Balouet, J.C.,, *The Toxicity of Commercial Jet Oils.* Environ. Research Sec A, 2002. **89**: p. 146-164.

15. Spicer, C.W., Murphy, M.J., Holdren, M.W., Myers, J.D., MacGregor, I.C., Holloman, C., James, R.R., Tucker, K., Zaborski, R.,, *Relate Air Quality and Other Factors to Comfort and Health Symptoms Reported by Passengers and Crew on Commercial Transport Aircraft*, in *American Society for Heating, Refrigerating, and Air Conditioning Engineers*. 2004.

16. Raub, J.A., Mattieu-Nolf, M., Hampson, N.B., Thom, S.R.,, *Carbon Monoxide Poisoning - A Public Health Perspective.* Toxicology, 2000. **145**: p. 1-14.

17. Sedda, A.F., Rossi, G., *Death Scene Evaluation in a Case of Fatal Accidental Carbon Monoxide Toxicity.* Forensic Science International, 2006. **164**: p. 164-167.

18. United States. National Air Pollution Control Administration., *Air quality criteria for carbon monoxide*. National Air Pollution Control Administration publication. 1970, Washington;: [For sale by the Supt. of Docs. 1 v. (various pagings).

19. Mousavi, P.W., D., Grant, C.S., Oxenham, W., Hauser, P.J.,, *Measuring Thermal Degradation of a Polyol Ester Lubricant in Liquid Phase.* Ind. Eng. Chem. Res., 2005. **44**: p. 5455-5464.

20. Mousavi, P., Wang, D., Grant, C.S., Oxenham, W., Hauser, P.J.,, *Effects of Antioxidants on the Thermal Degradation of a Polyol Ester Lubricant using GPC.* Ind. Eng. Chem. Res., 2006. **45**: p. 15-22.

21. Smith, J.R., Nagatomi, E., Waddington, D.J.,, *The Autoxidation of Simple Esters: Towards an Understanding of the Chemistry of Degradation of Polyol Esters Used as Lubricants.* J. of the Japan Petro. Inst., 2003. **46**: p. 1-14.

22. Siouris, S., Wilson, C.W.,, *Thermodynamic Properties of Pentaerythritol-based Species Involved in Degradation of Aviation Gas Turbine Lubricants.* Ind. Eng. Chem. Res., 2010. **49**: p. 12294-12301.

23. Bartl, P., Volkl, C., Kaiser, M.,, *Chemical Characterization of Polyol Ester Aviation Lubricant Residues.* J. Synthetic Lubrication, 2008. **25**: p. 1-16.
24. Keattch, C.J., Dollimore, D.,, *An Introduction to Thermogravimetry*. 2 ed. 1975: Heyden and Son Ltd.

25. Speyer, R.F., *Thermal Analysis of Materials*. 1994: Marcel Dekker, Inc.

26. *Thermogravimetric Analysis: A Beginner's Guide*, in *Frequently Asked Question*. 2010, PerkinElmer, Inc.: Waltham, MA. p. 1-19.

27. Crane, C.R., Sanders, D.C., Endecott, B.R., Abbott, J.K.,, *Inhalation Toxicology: III. Evaluation of Thermal Degradation Products from Aircraft and Automobile Engine Oils, Aircraft Hydraulic Fluid and Mineral Oil*, F.C.A. Institute, Editor. 1983, Office of Aviation Medicine: Oklahoma City, OK. p. 1-16.

28. *Aeroshell Turbine Oil 560*. 2008: Houston, TX. p. 1-8.

29. *Mobil Jet Oil II*. 2008: Fairfax, VA. p. 1-8.

30. Azarkish, H., Sarvari, S.M.H., Behzadmehr, A., *Optimum Geometry Design of a Longitudinal Fin with Volumetric Heat Generation Under the Influences of Natural Convection and Radiation.* Energy Conversion and Management, 2010. **51**: p. 1938-1946.

31. Rao, V.D., Naidu, S.V., Rao, B.G., Sharma, K.V., *Heat Transfer from a Horizontal Fin Array by Natural Convection and Radiation - A Conjugate Analysis.* International Journal of Heat and Mass Transfer, 2006. **49**: p. 3379-3391.

32. Dialameh, L., Yaghoubi, M., Abouali, O., *Natural Convection from an Array of Horizontal Rectangular Thick Fins with Short Length.* Applied Thermal Engineering, 2008. **28**: p. 2371-2379.

33. Neer, A.J., Andress, J.R., Haney, R.L., Overfelt, R.A., Prorok, B.C., Fergus, J.W., Mathison, L.C., *Preliminary Investigation into Thermal Degradation Behavior of Mobil Jet Oil II*, in *International Conference on Environmental Systems*. 2011, American Institute of Aeronautics and Astronautics: Portland, OR.

34. Haney, R.L., *Principal Component Analysis for Enhancement of Infrared Spectra Monitoring*, in *Materials Engineering*. 2011, Auburn University: Auburn, AL. p. 189.

35. Logerais, P.O., Girtan, M., Bouteville, A., *Influence of the Quartz Window in a Rapid Thermal Processing Apparatus.* Journal of Optoelectronics and Advanced Materials, 2006. **8**(1): p. 139-143.

36. Potze, W., *Radiation Heat Transfer in Axisymmetric Quartz Glass Tubes.* Journal of Quantitative Spectroscopy and Radiative Tranfer, 2004. **84**: p. 575-586.

37. Van Horn, K.R., *Aluminum: Properties, Physical Metallurgy, and Phase Diagrams*. Vol. 1. 1967, Metals Park, OH: American Society for Metals.

38. Kreith, F., *The CRC Handbook of Thermal Engineering*. 2000, Boca Raton, FL: CRC Press, LLC.

39. Janna, W.S., *Engineering Heat Transfer*. 2000, Boca Raton, FL: CRC Press, LLC.